Doctoral Dissertation(Censored)
博士論文 (要約)

Dynamic and Static Structural Analysis of Model Polymer Network Gel under Deformation
(モデルネットワークゲルの変形時における動的及び静的構造解析についての研究)

A Dissertation Submitted for the Degree of Doctor of Science

December 2021
令和 3 年 12 月博士 (理学) 申請

Department of Chemistry, Graduate School of Science,
The University of Tokyo

東京大学大学院理学系研究科化学専攻

Yui Tsuji
辻 優依

Abstract

My doctoral dissertation focuses on the structural analysis of model network gels under deformation, which was conducted with scattering methods with various irradiation sources, that is light, neutron, and X-ray.

The first topic is about the realization of model network gel. Polymer gels are usually heterogeneous, which means a random distribution of polymer segments (spatial heterogeneity). The heterogeneity is incorporated randomly into the gel network with the cross-linking reaction. Hence, the control of the heterogeneity is difficult. Spatial heterogeneity had been thought of as an inherent property of polymer gels because the cross-linking "freezes" the network structure. However, this preconception was broken from our previous study which reported the synthesis of the spatial homogeneous gel based on the simple and universal concept, i.e., the "bond percolation" concept. In this study, I removed the requirements to realize the bond percolation condition intentionally and introduced the different types of spatial heterogeneity into the gel network independently. The static and dynamic structure was quantified with various scattering methods, and the validity of the bond percolation concept was confirmed. In the following, I focused on the structural analysis model network gel synthesized based on the bond percolation concept.

The second and third topics are about the static structure of the model network gels under deformation, i.e., uniaxial elongation and uniaxial compression. In these sections, the structural analysis was conducted with small-angle scattering. In the previous studies, the spatial heterogeneous structure not only degrades the physical properties of gels such as mechanical strength and deformability but also disturbs the structural analysis with scattering methods due to the strong contribution of spatial heterogeneity for the scattering intensity. In these studies, I showed the effectiveness of the removal of spatial heterogeneity for the improvement of the mechanical properties of gels, and the obtained structure with fitting analysis gave information that is valuable to understand the deformation mechanism.

The final topic is the dynamic structural analysis of the model network gel under uniaxial compression with the quasi-elastic neutron scattering. Utilizing the labeling with the isotope as the feature of neutron scattering, I extracted the dynamics of the particular part of the network. Moreover, the orientation dependence of the dynamics was clarified. This might be due to the variation of the solvation structure with compression, however, it is not clear currently. Thus, further investigation should be conducted.

In this doctoral dissertation, I established the synthesis of the model network gels based on the simple and the non-constrained by polymer species concept and I focused on the understanding of the universal properties of gels through the structural analysis of the model network gels.

Contents

CHAPTER 1

General Introduction

1.1 The historical background of gel science
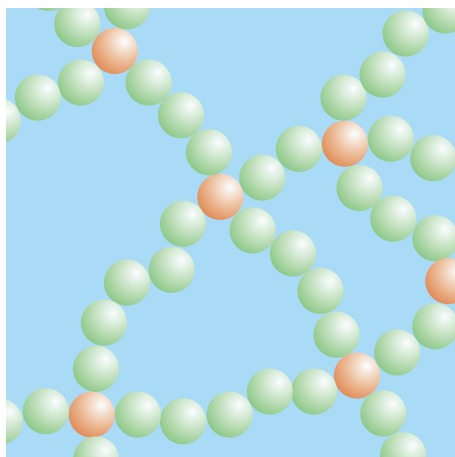
Figure 1.1: The schematic illustration of structure of gel (Green sphere: monomers, Red sphere: cross-linking points, pale blue of a background: a fluid)

Polymer gels are an elastic crosslinked network containing a fluid that fills the interstitial spaces of the network (Fig. 1.1) [1]. Gels look like a solid. However, there is a big difference compared with common solid materials such as metals or ceramics. Gels are soft and wet materials, which can deform largely and return to the initial shape when the applied force is released. Gels are ubiquitous materials and are seen widely in our daily life. Like boiled eggs, jelly, and meats, many foods are gels that originated from organisms. Industrially, many products are fabricated. In the medical field, a diaper or a sanitary item contains the gel as an absorber. And more, soft contact lenses which are made of gel have become common nowadays. In the environmental field, ion exchange resins such as ionized polystyrene gels are used to purify water.

Although gels have been familiar material for us in human history, history as

science is not so old. In the 19th century, "gel" was coined by Thomas Graham, the father of colloid chemistry, which is taken from gelatin. He described gel as "While the rigidity of the crystalline structure shuts out external expressions, the softness of the gelatinous colloid partakes of fluidity, and enables the colloid to become a medium for liquid diffusion, like water itself" [2]. In his description, the gel is classified into the type of colloids. At that time, the explicit definition of gel was not given. In actually, Lloyd wrote, "The colloid condition, the "gel," is one which is easier to recognize than to define" in 1926 [3]. Of course, from the point of view of present scientific knowledge, not all gels are colloids. However, there she also wrote, "Only one rule seems to hold for all gels, and that is that they must be built up from two components, one of which is a liquid at the temperature under consideration, and the other of which, the gelling substance proper, often spoken of as the gelator, is solid. The gel itself has the mechanical properties of a solid, i.e., it can maintain its form under the stress of its own weight, and under any mechanical stress, it shows the phenomenon of strain." This description is phenomenological but gets the point. Polymeric gels contain a liquid and show viscoelastic properties.

Later, more sophisticated definition was provided from Flory [4],

(1) Gels indicate the solid-like behavior. When gels deform, the response is elastic. Even if the plastic flow occurs for materials that are defined gels, it is limited for the case that the stress is only above a finite yield.
(2) Gels should have a continuous microscopic structure with macroscopic dimensions that is permanent on the time scale of observation of the system.

Moreover, Flory classfied gels into four types [4].

(1) Well-ordered lamellar structures, including gel mesophases.
(2) Covalent polymeric networks; completely disordered.
(3) Polymer networks formed through physical aggregation; predominantly disordered, but with regions of local order.
(4) Particulate, disordered structures.

In this dissertation, only gel of type (2), or chemically cross-linked polymer gels, is treated. As seen from these confusions of definition, a gel is not paid much attention as a subject of scientific analysis for a long time.

The turning point of gel science is the discovery of the volume phase transition. Dusek and Patterson predicted the volume phase transition in 1968 theoretically [5]. However, when the volume phase transition was experimentally observed was ten

years later than this theoretical prediction. In 1978, Tanaka discovered poly(acrylic amide) gels occurred during the volume phase transition when the composition of mixture solvent (water and acetone) was changed [6]. He reported that this occurred only for old gels, which were prepared about one month ago. This phenomenon was explained due to the hydrolysis of the polymer by Tanaka et al. later [7]. In 1984, Hirokawa et al. reported the non-ionic polymer gel indicated the discontinuous volume phase transition with temperature or a solvent composition [8]. This was the first example of the discontinuous change for the non-ionic polymer gel, poly(N-isopropylacrylamide) gel, and demonstrated the universality of the discontinuous volume phase transition of gels. This discovery gave a motive that the field of gel science was gotten intensive attention and developed extensively. Until then, since gels were complex to treat in physics, the number of studies had been limited. However, the discovery shed light on the physics of gel, and the study of functionalization of gels has become studied intensively [9–11]. Especially, many studies were conducted for gel sensors, actuators, and intelligent gels that changed their physical properties responding to external stimuli in the 1980s and 1990s [12, 13].

1.2 Model polymer network gel
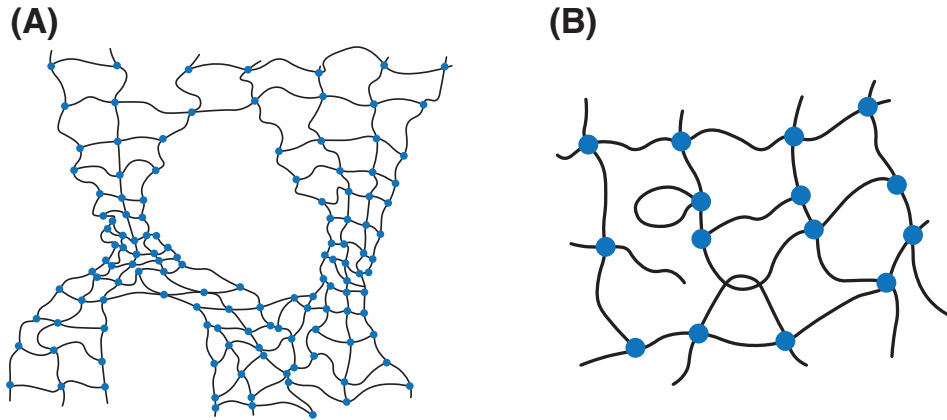
Figure 1.2: The schematic illustration of heterogeneities of gels. (A) Spatial heterongeneities, (B) topological heterogeneities.

Polymer gels, especially gels are obtained by free-radical crosslinking copolymerization, are usually "heterogeneous." Here, heterogeneous gel means that the network has the distribution of the mesh size (the length of polymer strands between crosslinkers) and topological and connectivity defects such as dangling chain ends, chains forming closed loops, and crosslinker-crosslinker shortcuts [14]. Former heterogeneity and later one is called spatial heterogeneityies(Fig. 1.2 (A)) and topo-

logical heterogeneities(Fig. 1.2 (B)), respectively. These heterogeneities lead to the deviation of the physical properties such as mechanical properties including mechanical strength and deformability [15–17], swelling and deswelling [18, 19], etc. from the expectation of theories. Because heterogeneities are incorporated into polymer network in an uncontrolled manner with the progress of a chemical reaction, the theoretical treatment of heterogeneities is also challenging. Therefore, researchers have attempted to develop the "model network" gels [20–23].

Hild defined the polymer network, which has below four features as the "ideal network" [24].

(i) All mesh size in the network is identical.
(ii) Polymer strands between crosslinkers should obey Gaussian statistics, which means the distribution of the probability of the distance of strand obeys Gaussian distribution.
(iii) The network should be homogeneous both macroscopically and microscopically. That is, the segment density and crosslink density are identical in the whole network.
(iv) The functionality of crosslinkers is constant in the whole network.
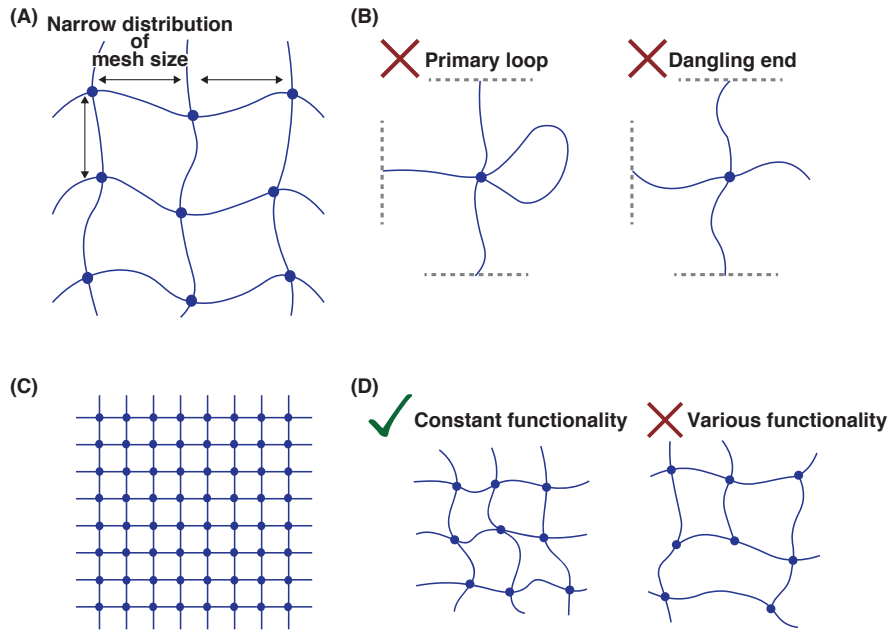
Figure 1.3: The schematic illustration of definition of model network gel. (A) Mesh sizes of nawwow molar mass distribution, (B) polymer strands connected by two different crosslinekers, (C) Constant density of crosslinkers and segments, (D) Constant functionality.

In reality, it is almost possible to attain the ideal network because real polymers have molecular weight distribution, and heterogeneities are incorporated with network formation. Thus, instead of an ideal network, the attainment of a "model network" has been pursued so far. A model network is defined as (Fig. 1.3)

(i) The mesh size should exhibit known length and a narrow molar mass distribution. Moreover, each polymer strand should be connected by its two ends to two different crosslinkers.

(ii) A model network should be homogeneous. That is, the segment density and crosslink density are identical in the whole network.

(iii) A model network should exhibit a known and constant functionality of crosslinkers.

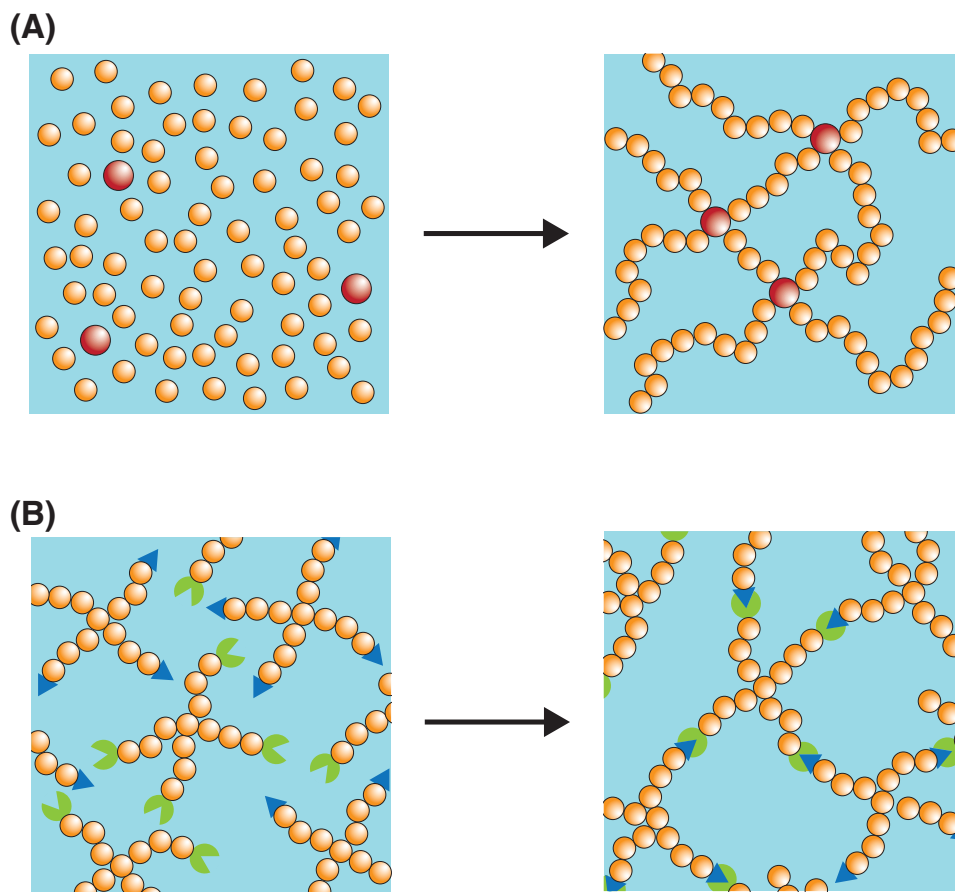## 1.3   Synthesis of polymer gels

Figure 1.4: The schematic illustration of synthesis of gels. (A) synthesis from monomers, and (B) synthesis from polymers.

The synthesis method for gels is divided into two types: from monomers and from polymers (Fig. 1.4).

When gels are synthesized from monomers, for instance, radical polymerization or polycondensation, gelation proceeds with polymerization and cross-linking process; this reaction is basically a random process, and the control of the network structure is impossible.

On the other hand, when gels are synthesized from polymers, such as end-linking or random cross-linking, only cross-linking reaction proceeds. Especially when gels are synthesized with an end-linking process with polymers, it is feasible to synthesize gels that fulfill the model network conditions, i.e., the control of the mesh size is easy and structural defects are suppressed to a certain extent. Many researchers attempted to fabricate model network gels from a combination of monodispersed multifunctional polymers and low-molecular-weight cross-linkers [24, 25]. However, even in these systems, the formation of topological defects is inevitable.

One of the most successful model network systems is Tetra-PEG gel [26]. Tetra-PEG gel was synthesized from crosslinking of two types of 4-arm star poly(ethylene glycol) (PEG) terminated with the mutually reactive functional group which can create a covalent bond with click reaction (Fig. 1.5). In this system, primary loops or loops in which odd numbers of tetra-arm polymers participate can be excluded effectively due to A-B type reaction between multifunctional polymers (Fig. 1.6 (A) and (C)) [27]. The reaction between the amino group and activated ester with N-hydroxysuccinimide or between the thiol and maleimide groups is widely used for Tetra-PEG gel.
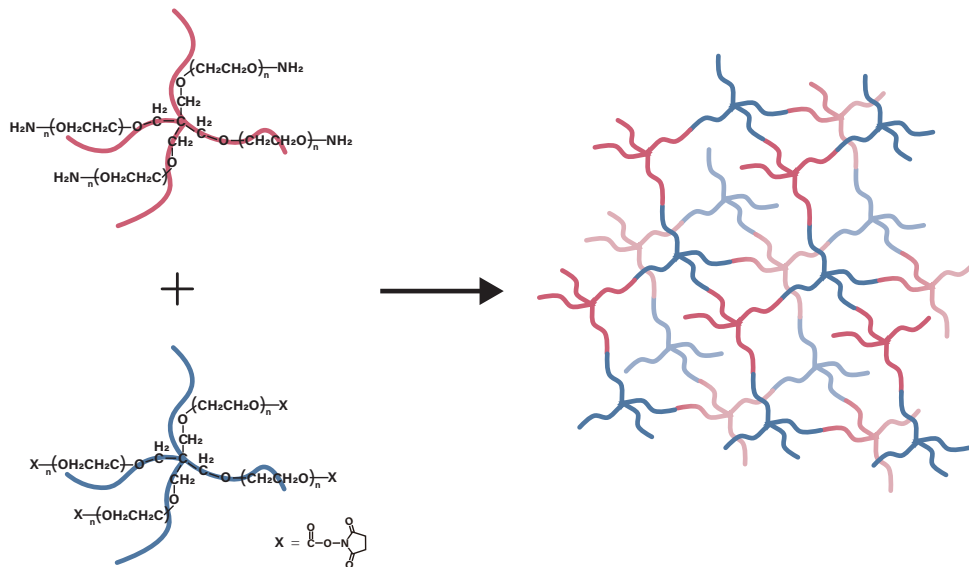

Figure 1.5: The schematic image of synthesis of Tetra-PEG gel. In this case, terminated groups are amine and activated ester N-hydroxysuccinimide.
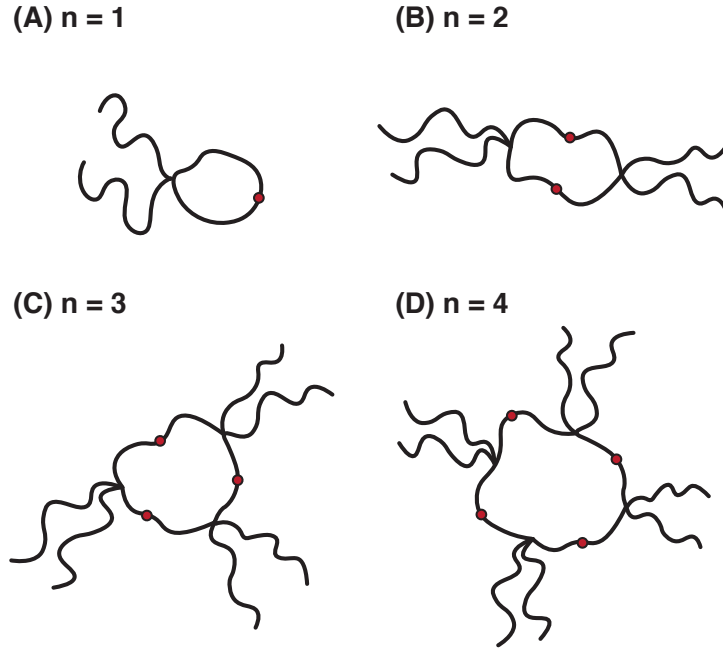
Figure 1.6: Loop structures formed from functinalized tetra-arm polymers in A-A type end-linking with (A) n=1, (B) n=2, (C) n=3, and (D) n=4 sets.

Since it is easy to prepare Tetra-PEG gel and adjust mesh size or crosslinking density, Tetra-PEG gel has been used for verification of various theories about elasticity, diffusion, osmotic pressure, and so on [28–34]. It was indicated that topological defects were less than conventional gel by the previous study [27]. However, as for spatial homogeneity, a certain level of heterogeneity was still observed with small-angle neutron scattering (SANS) [35]. It was suggested that the spatial heterogeneity was due to the aggregated structure of PEG, which is thought as the typical structure for PEG aqueous solution. [36, 37].

1.4 Highly homogeneous gel and "bond percolation" concept

So far, even the most successful example of model polymer network gels, Tetra-PEG gel, indicates the spatial heterogeneity somewhat. Gels are synthesized via the cross-linking process of polymer strands. In this process, it had been thought that the concentration fluctuation was fixed, which is the origin of the spatial heterogeneity [38]. Thus, spatial heterogeneity had believed as inherent nature of polymer gels and inevitable.

However, this preconception was broken recently by a report of the synthesis of the gel that is highly spatial homogeneous [39]. I call this spatial homogeneous gel the highly homogeneous gel. The highly homogeneous gel was prepared based on the "bond percolation" concept. "Bond percolation" is one type of percolation. The

percolation model is one of the lattice models and used for the description of the spreading of forest fires or contagious disease, other than gelation process [40]. The percolation model is composed of site latices and bond latices that connect each site. If an infinite cluster is formed with a connection of sites and bonds, the system "percolates." In the case of gelation, this means the sol-gel transition. Based on how sites and bonds are occupied, the percolation model can be classified. If all sites are occupied from the beginning, the percolation process is the progress of a random bond formation. This is called "bond percolation." On the other hand, when sites are occupied randomly, and the neighboring occupied sites are always connected into a cluster, this is called "site percolation." The model which is a combination of these two models is "site-bond percolation." In this model, site occupation is randomly progressed, and bond formations between adjacent occupied sites are also random.

The "bond percolation" concept is inspired by the "bond percolation" model. In the bond percolation model, all sites are preoccupied with mutually exclusive units in the initial state. The preparation condition for gel based on the "bond percolation" concept mimics this situation. When occupied site units are regarded as prepolymer units, the proceeding of mutual reaction between prepolymers during gelation reaction is considered as the bond percolation process. Satisfaction of this bond percolation concept leads to the uniform packed network with prepolymers, which avoids the incorporation of frozen spatial heterogeneity. That is, during the gelation process, we can avoid the formation of nano-voids or polymer aggregated domains that cause the concentration fluctuation.

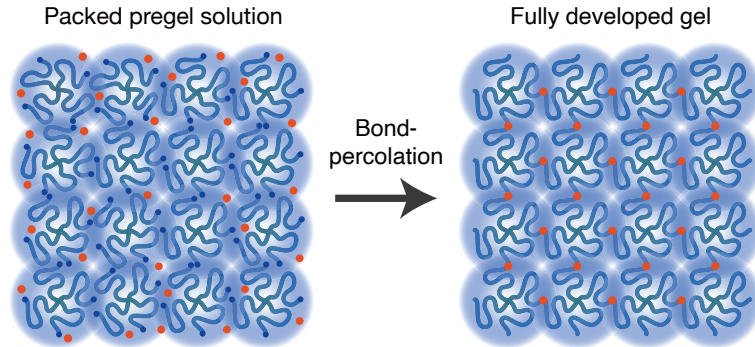Figure 1.7: The schematic illustration of structure of bond percolation condition [39].

In this study, the strategy to satisfy the bond percolation concept is to prepare gels at three conditions as below (Fig. 1.7).

(i) Using monodisperse star polymers. It is because polymers with multiple arms show a strong excluded volume effect that prevents other polymers from coming into the pervaded volume.

(ii) Preparing gels at a concentration well above its chain overlapping concentration c^*. It ensures that the star polymers uniformly and tightly fill the space as the bond percolation model assumes.

(iii) Choosing the high-affinity solvent to prepolymers. It is to prevent the segregation of polymer chains during cross-linking.

Here, as for condition (i), 4-arm star PEG (the weight averaged molecular weight M_w 20000) was used as a prepolymer. Condition (ii) was satisfied by preparing of the gel at a polymer concentration 12 weight % (wt%) because c^* of 4-arm star PEG of M_w 20000 is about 6wt% [29]. Condition (iii) was satisfied by using the dehydrated acetonitrile as a solvent, which shows excellent affinity to PEGs. The static and dynamic scattering indicated that the spatial heterogeneity was less negligible even at the range of wavelengths of light.

1.5   Outline of dissertation

My doctoral dissertation focuses on the structural analysis of model network gels under deformation, which was conducted with scattering methods with various irradiation sources, that is light, neutron, and X-ray. The structural analysis of gels under deformation has been disrupted so far due to spatial heterogeneity. Recently, as described above, the fabrication method of the highly spatial homogeneous gel has been established based on the bond percolation concept. In this dissertation, utilizing this concept, I describe the series of studies that I conducted in my doctoral course to clarify the deformation behavior of microscopic polymer strands in the gel network under various deformations. These studies contribute to elucidating the deformation mechanism of gels and giving the guideline for the reinforcement of gels.

In chapter 2, I introduce some theoretical background related to my doctoral research. Mainly, I focus on the principle of scattering phenomena and the mechanical properties of gels.

From chapter 3, I explain my doctoral research. First, in chapter 3, as based on the bond percolation concept introduced in this chapter, I demonstrated the intentional fabrication of the spatial heterogeneous gel distinguishing the kind of spatial heterogeneity, i.e., incorporated aggregation and nano-voids. This result also supported the validity of the bond percolation concept, that is, it is a universal concept for fabricating spatial homogeneous gels.

After chapter 4, I focus on the structural analysis of the model network gels fabricated based on the bond-percolation concept. In chapter 4, the static structural analysis of the model network gel under uniaxial elongation with small-angle X-ray scattering is introduced. In this study, I also tuned the reaction efficiency of the

terminated groups of prepolymers, or the fraction of the dangling chain, to examine the effect of bond defects on the network structure under elongation. From removing the spatial heterogeneity, it was clarified that the reaction efficiency affected elongation mechanical properties effectively. The static structure also drastically changed with decreasing reaction efficiency, and our result suggested that anisotropic 2D scattering profiles were related to the stretching of polymer strands.

In chapter 5, the static structural analysis of the model network gels under uniaxial compression with small-angle neutron scattering is introduced. In this study, the model network gels were partially labeled with deuterium utilizing the forte of neutron scattering. It was demonstrated that deuterium labeling makes us possible to extract structural information effectively. From model fitting, we could compare the microscopic polymer deformation and macroscopic bulk deformation.

In chapter 6, the dynamic structural analysis of the model network gels under uniaxial compression with quasi-elastic neutron scattering is introduced. Also here, isotope labeling was utilized. However, as different from the static neutron scattering, only the hydrogen labeled network was observed in this case. This study was the first observation of segmental dynamics of gels under deformation, as far as I know. Our experiment revealed that the segmental dynamics changed anisotropically with compression.

Finally, I describe the general conclusion summarizing the whole of my doctoral dissertation in chapter 7.

CHAPTER 2

Theoretical background

2.1 Basic theory of scattering

First, I introduce the basic theory for scattering techniques. In this section, static scattering (elastic scattering), quasi-elastic neutron scattering, and dynamic light scattering are introduced for the main techniques in my doctoral dissertation. The former two sections of this section are based on the book written by Roe [41]. The latter one is based on the books written by Berne and Pecora [42] and Johnson and Gabriel [43].

2.1.1 Static scattering

The scattering is divided into two processes. (1)The scattering occurs from each individual scatterers (Light: atoms, X-ray: electrons, and Neutron: nucleus). (2)The wave is scattered from each scatterer then interference each other. Strictly, the scattering indicates only phenomena (1). The combination of (1) and (2) is called diffraction. However, especially in small-angle scattering, the term "scattering" involves a combination of both (1) and (2).
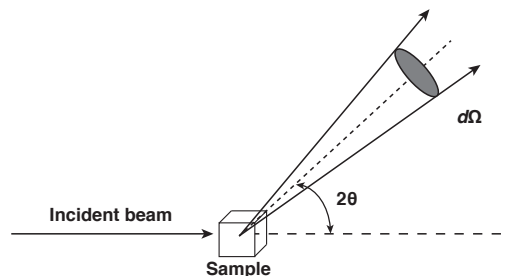

Figure 2.1: Schematic image of basic geometry of scattering.

The intensity of scattering is described as the flux J, which is measured as the amount of energy that is transmitted per unit solid angle per second. When the

scattered wave is regarded as a stream of particles, J is represented by the particle flux that is the number of photons or neutrons passing through a unit solid angle per second. J is proportional to the square of the amplitude A of the oscillating wave field, that is, the scattered wave here. The scattered wave is usually expressed with the complex number, then J is thus given by

$$J = |A|^2 = AA^* \tag{2.1}$$

Suppose the irradiated wave is J_0 (Fig. 2.1), J will increase or decrease in proportion with J_0. The quantity that we are really interested in is the ratio J/J_0 as a function of the scattering direction. Here, while the irradiated wave is the plane wave, the scattered wave is the spherical wave. Thus, the ratio of J/J_0 has a dimension of area per solid angle. This quantity is called the differential scattering cross-section

$$\frac{d\sigma}{d\Omega} = \frac{J}{J_0} \tag{2.2}$$

$d\sigma/d\Omega$ is also thought of as the probability that a photon or a neutron impinging on the sample is scattered into a unit solid angle in the given direction.
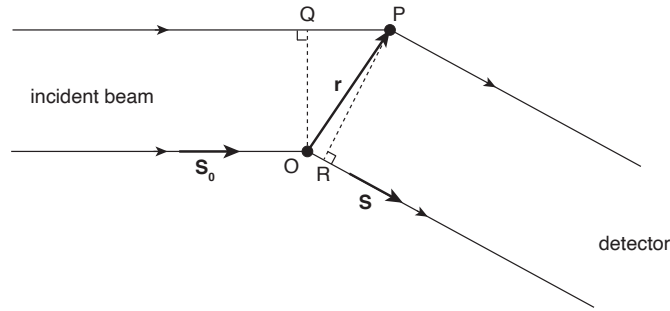
Figure 2.2: Schematic image of path length defferecne.

Now, the scattering from two points, O and P, is considered (Fig. 2.2). It is assumed that the scattering is coherent, and there is no phase change on scattering. The spherical wave scattered at O by particle 1 of traveling in the x direction can be written as

$$A_1(x, t) = \frac{A_0}{R_D} b \exp[i2\pi(\nu t - x/\lambda)] \tag{2.3}$$

where R_D, ν, t, and λ are the distance between scattering point and observed point, frequency, time, and wavelength, respectively. A_0 is the amplitude of the incident radiation and b is the scattering length that expresses the efficiency of scattering by the particle, which depends on the source of irradiation beam. The phase difference $\Delta\phi$ between the two waves scattered at O and P and arriving at the detector depends

only on the path length difference δ between the two rays. It is written as

$$\Delta\phi = \frac{2\pi\delta}{\lambda} \tag{2.4}$$

When the position of P is located as vector $\boldsymbol{r}$ from O, since $QP = \boldsymbol{S_0} \cdot \boldsymbol{r}$ and $OR = \boldsymbol{S} \cdot \boldsymbol{r}$, $\Delta\phi$ can be described as

$$\Delta\phi = \frac{2\pi}{\lambda}(\boldsymbol{S_0} \cdot \boldsymbol{r} - \boldsymbol{S} \cdot \boldsymbol{r}) = -\boldsymbol{q} \cdot \boldsymbol{r} \tag{2.5}$$

where $\boldsymbol{S_0}$ and $\boldsymbol{S}$ are unit vectors and $\boldsymbol{q}$ is defined as

$$\boldsymbol{q} = \frac{2\pi}{\lambda}(\boldsymbol{S} - \boldsymbol{S_0}) \tag{2.6}$$

$\boldsymbol{q}$ is called the scattering vector, which is related to the scattering angle 2θ by

$$|\boldsymbol{q}| = q = \frac{4\pi\sin\theta}{\lambda} \tag{2.7}$$

Thus, spherical wave scattered at P by particle 2 can be written as

$$A_2(x,t) = A_1(x,t)\exp(i\Delta\phi) = \frac{A_0}{R_D}b\exp[i2\pi(\nu t - x/\lambda)]\exp(-\boldsymbol{q} \cdot \boldsymbol{r}) \tag{2.8}$$

The wave reached the detector is conbination of wave $A(x,t)$, which is described by the sum of $A_1(x,t)$ and $A_2(x,t)$:

$$\begin{aligned} A(x,t) &= A_1(x,t) + A_2(x,t) = A_1(x,t)\exp(i\Delta\phi) \\ &= \frac{A_0}{R_D}b\exp[i2\pi(\nu t - x/\lambda)][1 + \exp(-i\boldsymbol{q} \cdot \boldsymbol{r})] \end{aligned} \tag{2.9}$$

From (2.1), the scattered flux is evaluated as

$$J(\boldsymbol{q}) = A(x,t)A^*(x,t) = \frac{A_0^2}{R_D^2}b^2[1 + \exp(-i\boldsymbol{q} \cdot \boldsymbol{r})][1 + \exp(i\boldsymbol{q} \cdot \boldsymbol{r})] \tag{2.10}$$

Here, the factors $\exp[i2\pi(\nu t - x/\lambda)]$ and $\exp[-i2\pi(\nu t - x/\lambda)]$ canceled out. Thus, it is enough to write $A(x,t)$ as

$$A(\boldsymbol{q}) = \frac{A_0}{R_D}b[1 + \exp(-i\boldsymbol{q} \cdot \boldsymbol{r})] \tag{2.11}$$

When there is identical n scatterers, eq.(2.11) can be easily generalized to

$$A(\boldsymbol{q}) = \frac{A_0}{R_D}b\sum_{j=1}^{n}\exp(-i\boldsymbol{q} \cdot \boldsymbol{r}_j) \tag{2.12}$$

where $\boldsymbol{r}_j$ is the position of the jth scatterer relative to an arbitrary origin. If there are numerous scatterers and scatterers continuously dispersed in space in the sample, the summation of eq.(2.12) can be replaced with an integral.

$$A(\boldsymbol{q}) = \frac{A_0}{R_D}b\int_V n(\boldsymbol{r})\exp(-i\boldsymbol{q} \cdot \boldsymbol{r})d\boldsymbol{r} \tag{2.13}$$

where $n(\boldsymbol{r})d\boldsymbol{r}$ represents to the number of scatterers within a volume element $d\boldsymbol{r} = dxdydz$ around $\boldsymbol{r}$ and V is the scattering volume, which is the illuminated volume. eq.(2.13) indicates that $A(\boldsymbol{q})$ is proportional to the three-dimensional Fourier transform of $n(\boldsymbol{r})$. More generally, eq (2.13) can be writen as

$$A(\boldsymbol{q}) = \frac{A_0}{R_D} \int_V \rho(\boldsymbol{r}) \exp(-i\boldsymbol{q} \cdot \boldsymbol{r})d\boldsymbol{r} \tag{2.14}$$

where $\rho(\boldsymbol{r})$ is the scattering length density distribution. When we consider the scattering measurement, the position of scatterers, that is $\rho(\boldsymbol{r})$ may change due to the thermal motion of scatterers during a time period of measurement. Thus measured scattered intensity is averaged over time. In an equibrium system which obeys the ergodic hypothesis, the time average and the ensemble are equivalrnt. Hence, the total scattered intensity $I(q)$

$$I(q) = \frac{I_1}{R_D^2} \frac{d\sigma}{d\Omega} = \langle |A(\boldsymbol{q})|^2 \rangle = \frac{I_1}{R_D^2} \left\langle |\int_V \rho(\boldsymbol{r}) \exp(-i\boldsymbol{q}\boldsymbol{r})d\boldsymbol{r}|^2 \right\rangle \tag{2.15}$$

where $I_1 = A_0^2$ is the irradiated radiation intensity and $\langle \cdots \rangle$ denotes the ensemble average.

So far, an assembly of nuclei of a single element is considered. In neutron scattering, the scattering intensity depends on the kind of nucleus, and the neutron has spin $1/2$. The neutron interacts with spin of the nucleus. Therefore, the scattering length in the sample is not described by the identical value b excepted in the case that if the sample is isotopically pure and the nuclear spin is zero. When spin of a nucleus is i, each nucleus take one of two different scattering density b^+ or b^- depending on the spin direction. The total spin due to the interaction between nucleus and neutron is either $i + 1/2$ or $i - 1/2$. Therefore, the probability that the scattering length b^+ is realized as

$$f^+ = \frac{2i + 2}{4i + 2} = \frac{i + 1}{2i + 1} \tag{2.16}$$

and for b^- as

$$f^- = \frac{2i}{4i + 2} = \frac{i}{2i + 1} \tag{2.17}$$

This random variability indicates that scattering intensity in neutron scattering contains not only a component that reflected the structure as usual but also another component that does not have structural information arising from the scattering length randomness. Now, I consider the system the assembly of the same atoms, but the scattering length b varies from nucleus to nucleus due to either the nonzero spin or the presence of isotopes. In this case, eq (2.12) can be written as

$$A(\boldsymbol{q}) = \frac{A_0}{R_D} \sum_{j=1}^{n} b_j \exp(-i\boldsymbol{q} \cdot \boldsymbol{r}_j) \tag{2.18}$$

and

$$\frac{\partial\sigma}{\partial\Omega} = \sum_{j,k}\langle b_j b_k\rangle \exp[-i\boldsymbol{q}\cdot(\boldsymbol{r}_j - \boldsymbol{r}_k)] \tag{2.19}$$

where $\langle b_j b_k\rangle$ is the expectation value of $b_j b_k$ in view of the random variability of b_j and b_k. In the case for j equal to k,

$$\langle b_j b_k\rangle = \langle b_j^2\rangle = \langle b^2\rangle \tag{2.20}$$

while for $j \neq k$,

$$\langle b_j b_k\rangle_{j\neq k} = \langle b_j\rangle\langle b_k\rangle = \langle b\rangle^2 \tag{2.21}$$

bacause there is no correlation between the values of b_j and b_k. With eq (2.20) and eq (2.21) it can be written as

$$\langle b_j b_k\rangle = \langle b\rangle^2 + \delta_{j,k}(\langle b^2\rangle - \langle b\rangle^2) \tag{2.22}$$

where $\delta_{j,k}$ is the Kronecker delta, which is equal to 1 if $j = k$ and equal to 0 otherwise. Then, substituting eq (2.22) into eq (2.19) gives

$$\frac{\partial\sigma}{\partial\Omega} = \langle b\rangle^2 \sum_{j,k}\exp[-i\boldsymbol{q}\cdot(\boldsymbol{r}_j - \boldsymbol{r}_k)] + n(\langle b^2\rangle - \langle b\rangle^2) \tag{2.23}$$

The first term of eq (2.23) is equal the scattering intensity in the case of that all the nuclei had the identical scattering length equal to the average $\langle b\rangle$. The second term does not depend on the position of the atoms, thus, does not contain structural information of the sample. This term is simply proportional to the variance $\langle b^2\rangle - \langle b\rangle^2 = \langle(b-\langle b\rangle)^2\rangle$, which indicates that it arises from the fluctuation of the scattering lengths. These two terms are called the coherent and incoherent components of the intensity, respectively. The coherent and incoherent scattering lengths of an element or an isotope are defined as

$$b_{\text{coh}} = \langle b\rangle \tag{2.24}$$

$$b_{\text{inc}} = (\langle b^2\rangle - \langle b\rangle^2)^{1/2} \tag{2.25}$$

Form factor and Structure factor

If one molecule are composed of n scatterers, eq (2.15) becomes the scattered intensity of one molecules;

$$I(q) = \frac{I_1}{R_D^2}\left\langle \int_V \int_V \rho(\boldsymbol{r}_i)\rho(\boldsymbol{r}_j)\exp(-i\boldsymbol{q}\cdot(\boldsymbol{r}_i - \boldsymbol{r}_j)d\boldsymbol{r}\right\rangle = \frac{I_1 n^2}{R_D^2}P(q) \tag{2.26}$$

Here, $P(q)$ is called the form factor and defined as

$$P(q) = \frac{1}{n^2} \left\langle \int_V \int_V \rho(\boldsymbol{r}_i)\rho(\boldsymbol{r}_j) \exp(-i\boldsymbol{q} \cdot (\boldsymbol{r}_i - \boldsymbol{r}_j) d\boldsymbol{r} \right\rangle \tag{2.27}$$

eq.(2.26) holds in only dilute condition. If the system is in dence condition, the inteference between molecules becomes non-negligible.

Here, I consider N particles system, which each particles are composed with n scatterers. The position of particle j is defined as $\boldsymbol{R} = \boldsymbol{R}_j + \boldsymbol{r}$. In this case, the scattering intensity is discribed as

$$I(q) = \frac{I_1}{R_D^2} \left\langle |\sum_{j=1}^{N} \exp(-i\boldsymbol{q} \cdot \boldsymbol{R}_j) \int_V \rho(\boldsymbol{r}) \exp(-i\boldsymbol{q} \cdot \boldsymbol{r}) d\boldsymbol{r}|^2 \right\rangle = \frac{I_1}{R_D^2} n^2 N P(q) S(q) \tag{2.28}$$

where $S(q)$ is called structure factor and defined as

$$S(q) = \frac{1}{N} \left\langle \sum_{j,k}^{N} \exp[-i\boldsymbol{q} \cdot (\boldsymbol{R}_j - \boldsymbol{R}_k)] \right\rangle \tag{2.29}$$

This equation expresses the interference effect.

2.1.2 Inelastic neutron scattering

In inelastic neutron scattering, we observe the double-differential scattering cross section $\partial^2 \sigma / \partial\Omega\partial\omega$, which is the probability that an incident neutron with wave vector $\boldsymbol{k}_0$ and energy E_0 is scattered by a scattering angle 2θ into a solid angle element $d\Omega$ and an energy interval between E_1 and $E_1 + dE$. Here E and $\boldsymbol{k}_1$ are the energy and wave vecor of scattered neutron, respectively. The momentum transfer $\hbar\boldsymbol{q}$ and energy transfer ΔE of neutron is described as

$$\hbar\boldsymbol{q} = \hbar(\boldsymbol{k}_1 - \boldsymbol{k}_0) \tag{2.30}$$

$$\Delta E = \hbar\omega = E_1 - E_0 = \frac{\hbar^2}{2m}(k_1^2 - k_0^2) \tag{2.31}$$

where ω is the change in the angular frequency on scattering (i.e., $\omega = \omega_1 - \omega_0$, where ω_0 and ω_1 are the angular frequency of incident and scattered neutrons.) Here, it should be noted that the magnitude of scattering vector q is no longer determined solely by the scattering angle 2θ because of $k_0 \neq k_1$. In inelastic scattering, q is described as

$$q^2 = k_0^2 + k_1^2 - 2k_0 k_1 \cos 2\theta \tag{2.32}$$

The double-differential scattering cross section $\partial^2\sigma/\partial\Omega\partial\omega$ is written as

$$\frac{\partial^2\sigma}{\partial\Omega\partial\omega} = \frac{k_1}{k_0}\frac{1}{2\pi}\sum_j\sum_k b_j b_k \int_{-\infty}^{\infty}\langle\exp[-i\boldsymbol{q}\cdot\boldsymbol{r}_j(t)]\exp[i\boldsymbol{q}\cdot\boldsymbol{r}_k(0)]\rangle\exp(i\omega t)dt \quad (2.33)$$

with the position $\boldsymbol{r}_j(t)$ of all nuclei ($j = 1,\ldots,N$) on function of time t. In the following, for simplicity, it is assumed that the scattering system consists of nuclei of a single element, and the element contains a single isotope whose nuclear spin is zero. Thus, the scattering length of eq (2.33) b_j can be written as same numerical value b.

Here, the intermediate scattering function $F(\boldsymbol{q},t)$ and the time-dependent pair correlation function (or van Hove correlation function) $G(\boldsymbol{r},t)$ are defined as

$$F(\boldsymbol{q},t) = \frac{1}{N}\sum_{j=1}^{N}\sum_{k=1}^{N}\langle\exp[-i\boldsymbol{q}\cdot\boldsymbol{r}_j]\exp[i\boldsymbol{q}\cdot\boldsymbol{r}_k]\rangle \quad (2.34)$$

$$G(\boldsymbol{r},t) = \frac{1}{(2\pi)^3}\int F(\boldsymbol{q},t)\exp(i\boldsymbol{q}\cdot\boldsymbol{r})d\boldsymbol{q} \quad (2.35)$$

respectively. Hence, eq (2.33) can be written as

$$\begin{aligned}\frac{\partial^2\sigma}{\partial\Omega\partial\omega} &= \frac{k_1}{k_0}b^2 N\frac{1}{2\pi}\int_{\infty}^{\infty}F(\boldsymbol{q},t)\exp(i\omega t)\\ &= \frac{k_1}{k_0}b^2 N\frac{1}{2\pi}\int_{\infty}^{\infty}\int_V G(\boldsymbol{r},t)\exp[-i(\boldsymbol{q}\cdot\boldsymbol{r}-\omega t)]d\boldsymbol{r}dt\end{aligned} \quad (2.36)$$

By defining the dynamic structure factor $S(\boldsymbol{q},\omega)$ as

$$\begin{aligned}S(\boldsymbol{q},\omega) &= \frac{1}{2\pi}\int_{\infty}^{\infty}F(\boldsymbol{q},t)\exp(i\omega t)dt\\ &= \frac{1}{2\pi}\int_{\infty}^{\infty}\int_V G(\boldsymbol{r},t)\exp[-i(\boldsymbol{q}\cdot\boldsymbol{r}-\omega t)]d\boldsymbol{r}dt\end{aligned} \quad (2.37)$$

eq (2.33) can be written in the more compact form as

$$\frac{\partial^2\sigma}{\partial\Omega\partial\omega} = \frac{k_1}{k_0}b^2 N S(\boldsymbol{q},\omega) \quad (2.38)$$

These three function ($F(\boldsymbol{q},t)$, $G(\boldsymbol{r},t)$, $S(\boldsymbol{q},\omega)$) are related to each other through Fourier transforms in space or in time (Fig. 2.3). It should be noted that the dimention of $F(\boldsymbol{q},t)$, $G(\boldsymbol{r},t)$, and $S(\boldsymbol{q},\omega)$ is dimentionless, [volume^{-1}], and [time], respectively.

From eq (2.35) and eq (2.34), the time-dependent pair correlation function is

$$G(\boldsymbol{r},t) \quad\longleftrightarrow\quad F(\boldsymbol{q},t) \quad\longleftrightarrow\quad S(\boldsymbol{q},\omega)$$

Fourier transform in space   **Fourier transform in time**
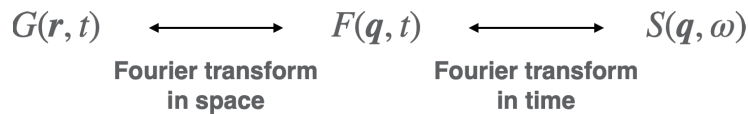
Figure 2.3: Fourier transformation relationships among $F(\boldsymbol{q},t)$, $G(\boldsymbol{r},t)$, and $S(\boldsymbol{q},\omega)$

written as

$$G(\boldsymbol{r},t) = \frac{1}{N}\sum_{j=1}^{N}\sum_{k=1}^{N}\frac{1}{(2\pi)^3}\int\langle\exp(-i\boldsymbol{q}\cdot\boldsymbol{r}_j(t))\exp(i\boldsymbol{q}\cdot\boldsymbol{r}_k(0))\rangle\exp(i\boldsymbol{q}\cdot\boldsymbol{r})d\boldsymbol{q} \quad (2.39)$$

With the following relationship

$$\delta(\boldsymbol{r}-\boldsymbol{a}) = \frac{1}{(2\pi)^3}\int\exp(-i\boldsymbol{q}\cdot\boldsymbol{a})\exp(i\boldsymbol{q}\cdot\boldsymbol{r})d\boldsymbol{q} \quad (2.40)$$

eq (2.39) can be rewritten as

$$G(\boldsymbol{r},t) = \frac{1}{N}\sum_{j=1}^{N}\sum_{k=1}^{N}\langle\delta[\boldsymbol{r}-\boldsymbol{r}_j(t)-\boldsymbol{r}_k(0)]\rangle \quad (2.41)$$

When the nuclei are equivalent, the sum over j in eq (2.41) gives the same value irrespective of k for fixed k. Thus, the sum over k becomes N times the term with $k = 1$. Then,

$$G(\boldsymbol{r},t) = \sum_{j=1}^{N}\langle\delta[\boldsymbol{r}-\boldsymbol{r}_j(t)-\boldsymbol{r}_1(0)]\rangle \quad (2.42)$$

$\boldsymbol{r}_1(0)$ is taken as the origin, $G(\boldsymbol{r},t)d\boldsymbol{r}$ can be interpreted as the probability that when a particle is at the origin at time $t = 0$, any particle is in the volume $d\boldsymbol{r}$ at position $\boldsymbol{r}$ at time t. Eq (2.42) can be splitted into the self (s) and the distinct (d) part as

$$G(\boldsymbol{r},t) = G_{\rm s}(\boldsymbol{r},t) + G_{\rm d}(\boldsymbol{r},t) \quad (2.43)$$

where $G_{\rm s}(\boldsymbol{r},t)$ is the probability that the particle which was at position $\boldsymbol{r} = 0$ at time $t = 0$ will be at position $\boldsymbol{r}$ at time $t = 0$ and $G_{\rm d}(\boldsymbol{r},t)$ is the probability that after seeing a particle at the origin and time $t = 0$, we see different particle at $\boldsymbol{r} = 0$.

In the limit $t \rightarrow \infty$, $G_{\rm s}(\boldsymbol{r},t)$ and $G_{\rm d}(\boldsymbol{r},t)$ become independent of $\boldsymbol{r}$, and the behavior at $\boldsymbol{r} \rightarrow \infty$ is same as that at $t \rightarrow \infty$. Thus,

$$\lim_{r\to\infty}G_{\rm s}(\boldsymbol{r},t) = \lim_{t\to\infty}G_{\rm s}(\boldsymbol{r},t) = \frac{1}{V} \approx 0 \quad (2.44)$$

$$\lim_{r\to\infty}G_{\rm d}(\boldsymbol{r},t) = \lim_{t\to\infty}G_{\rm d}(\boldsymbol{r},t) \approx \langle n\rangle \quad (2.45)$$

As described in the previous section, in static neutron scattering, the scattering of neutrons from an assemblage of atomic nuclei consists of coherent and incoherent components. Therefore, also in inelastic scattering, scattered neutron consists of coherent and incoherent component. Here, I consider the system coitaining a single type of element. Reflecting the random variability in the scattering length b of the

individual nucleis, eq (2.33) can be written as

$$\frac{\partial^2 \sigma}{\partial \Omega \partial \omega} = \frac{k_1}{k_0} \frac{1}{2\pi} \sum_j \sum_k \langle b_j b_k \rangle \int_{-\infty}^{\infty} \langle \exp[-i\boldsymbol{q} \cdot \boldsymbol{r}_j(t)] \exp[i\boldsymbol{q} \cdot \boldsymbol{r}_k(0)] \rangle \exp(i\omega t) dt \quad (2.46)$$

where $\langle b_j b_k \rangle$ is the expectaiton value of $b_j b_k$. The summation in eq (2.46) is separated into two sum depended on whether j equals to k.

$$
\begin{aligned}
\frac{\partial^2 \sigma}{\partial \Omega \partial \omega} = & \frac{k_1}{k_0} \frac{\langle b^2 \rangle}{2\pi} \sum_j \int_{-\infty}^{\infty} \langle \exp[-i\boldsymbol{q} \cdot \boldsymbol{r}_j(t)] \exp[i\boldsymbol{q} \cdot \boldsymbol{r}_j(0)] \rangle \exp(i\omega t) dt \\
& + \frac{k_1}{k_0} \frac{\langle b \rangle^2}{2\pi} \sum_{j \neq k} \int_{-\infty}^{\infty} \langle \exp[-i\boldsymbol{q} \cdot \boldsymbol{r}_j(t)] \exp[i\boldsymbol{q} \cdot \boldsymbol{r}_k(0)] \rangle \exp(i\omega t) dt
\end{aligned}
\quad (2.47)
$$

The incoherent and incoherent scattering length are defined in eq (2.24) and eq (2.25). Thus, from substituting both into eq (2.47), it can be rewritten as

$$
\begin{aligned}
\frac{\partial^2 \sigma}{\partial \Omega \partial \omega} = & \frac{k_1}{k_0} \frac{b_{\text{inc}}^2}{2\pi} \sum_j \int_{-\infty}^{\infty} \langle \exp[-i\boldsymbol{q} \cdot \boldsymbol{r}_j(t)] \exp[i\boldsymbol{q} \cdot \boldsymbol{r}_j(0)] \rangle \exp(i\omega t) dt \\
& + \frac{k_1}{k_0} \frac{b_{\text{coh}}^2}{2\pi} \sum_j \sum_k \int_{-\infty}^{\infty} \langle \exp[-i\boldsymbol{q} \cdot \boldsymbol{r}_j(t)] \exp[i\boldsymbol{q} \cdot \boldsymbol{r}_k(0)] \rangle \exp(i\omega t) dt
\end{aligned}
\quad (2.48)
$$

The first term in eq (2.48) is called the incoherent scattering component and gives information about the motions of individual nuclei but does not give their correlation with other nuclei. On the other hand, the second term, the coherent scattering component, contains information about the relative motion between nuclei j and k, including the contribution from the same nuclei case $j = k$. From the definition of the time-dependent pair correlation function $G(\boldsymbol{r}, t)$ and self-part of that $G_{\text{s}}(\boldsymbol{r}, t)$, the coherent and incoherent conponent of the double differential scattering cross section can be described as

$$\left(\frac{\partial^2 \sigma}{\partial \Omega \partial \omega} \right)_{\text{coh}} = \frac{k_1}{k_0} \frac{N b_{\text{inc}}^2}{2\pi} \int_{-\infty}^{\infty} \int G_{\text{s}}(\boldsymbol{r}, t) \exp -(\boldsymbol{q} \cdot \boldsymbol{r} - \omega t) d\boldsymbol{r} dt \quad (2.49)$$

and

$$\left(\frac{\partial^2 \sigma}{\partial \Omega \partial \omega} \right)_{\text{inc}} = \frac{k_1}{k_0} \frac{N b_{\text{coh}}^2}{2\pi} \int_{-\infty}^{\infty} \int G(\boldsymbol{r}, t) \exp -(\boldsymbol{q} \cdot \boldsymbol{r} - \omega t) d\boldsymbol{r} dt \quad (2.50)$$

respectively. The intermediate scattering function $F(\boldsymbol{q}, t)$ and the dynamic structure factor $S(\boldsymbol{q}, \omega)$ can also be separated into their respective "self" and "distinct" parts.

$$F(\boldsymbol{q}, t) = F_{\text{s}}(\boldsymbol{q}, t) + F_{\text{d}}(\boldsymbol{q}, t) \quad (2.51)$$

$$S(\boldsymbol{q}, \omega) = S_{\text{s}}(\boldsymbol{q}, \omega) + S_{\text{d}}(\boldsymbol{q}, \omega) \quad (2.52)$$

It is noted that the "self" part $F_{\text{s}}(\boldsymbol{q}, t)$ or $S_{\text{s}}(\boldsymbol{q}, \omega)$ is associated with the incoherent

scattering cross section like

$$\left(\frac{\partial^2 \sigma}{\partial\Omega\partial\omega}\right)_{\text{inc}} = \frac{k_1}{k_0}b_{\text{inc}}^2 N S_{\text{s}}(\boldsymbol{q},\omega) \tag{2.53}$$

Practically, it is difficult to distinguish between incoherent and coherent scattering. However, most polymers contain rich hydrogen atoms and the scattering is predominantly incoherent because hydrogen atom has a large contribution for incoherent scattering due to the nonzero spin. The coherent scattering of polymers is usually concentrated in a few Bragg peaks or broader maxima in the wider q region. If we avoid these q regions, the observed scattering intensity is almost incoherent. In such cases, the scattering results are composed of the self motions of hydrogen atoms, which makes it feasible to interpret the results considerably.

2.1.3 Dynamic light scattering (Quasi-elastic light scattering)

The dynamic scattering is the method for examining the dynamics such as the translational diffusion coefficient D_{T} in the solution from the fluctuation of the scattering light due to the thermal motion. D_{T} gives information about molecular weight or hydrodynamic molecular diameter combined with some relationship.

To extract the dynamical properties from the fluctuation of the scattering light, I consider the time-dependent correlation function. Here, A is a property that depends on the positions and momenta of all the particles in the system. Because of their thermal motion, the particles move around and collide. Thus, their positions and momenta vary with time and also A. Although their movement obeys the Schrödinger's equation, it looks random motion. If time T is large enough compared to the period of fluctuation, the average of A becomes independent of when the measurement is initiated.

$$\langle A \rangle_T = \lim_{T\to\infty}\frac{1}{T}\int_0^T dt A(t) \tag{2.54}$$

I consider the property between time t and $t+\tau$. As τ increases the defference between $A(t)$ and $A(t+\tau)$ becomes more likely nonzero. This means that $A(t)$ and $A(t+\tau)$ are correlated when τ is small. This correlation is lost if τ becomes large enough compared with the period of the fluctuation. The autcorrelation function of A which expresses this correlatio is defined as

$$\langle A(0)A(\tau) \rangle_T = \lim_{T\to\infty}\frac{1}{T}\int_0^T dt A(t)A(t+\tau) \tag{2.55}$$

I consider the property A whose average $\langle A \rangle$ is 0 and fluctuation is between positive and negative. In this case, $A(0)A(\tau)$ can take the negative value and $\langle A(0)A(\tau)\rangle$ becomes smaller due to the cancellation between positive and negative terms com-

pared with $A(0)^2$.

$$\langle A(0)^2 \rangle_T \geq \langle A(0)A(\tau) \rangle_T \tag{2.56}$$

Thus, the autocorrelation function either remains equal to its initial value for all time τ or decays from its initial value, in which case A is a constant of the motion. For large τ compared to the characteristic time for the fluctuation of A which is nonconserved and nonperiodic property, $A(t)$ and $A(t + \tau)$ become totally uncorrelated.

$$\lim_{\tau \to \infty} \langle A(0)A(\tau) \rangle_T = \langle A(0) \rangle_T \langle A(\tau) \rangle_T = \langle A \rangle_T^2 \tag{2.57}$$

Thus, the time correlation function decays from $\langle A^2 \rangle$ to $\langle A \rangle^2$ with time.

In many cases, the autocorrelation function decays like a single exponential as

$$\langle A(0)A(\tau) \rangle_T = \langle A \rangle_T^2 + [\langle A^2 \rangle_T - \langle A \rangle_T^2] \exp\left(-\frac{\tau}{\tau_r}\right) \tag{2.58}$$

where τ_r is the relaxation time or the correlation time of the property. The deviation of the instantaneous value of $A(t)$ from its average value is defined as

$$\delta A(t) \equiv A(t) - \langle A \rangle_T \tag{2.59}$$

Thus,

$$\langle \delta A(0) \delta A(\tau) \rangle_T = \langle A(0)A(\tau) \rangle_T - \langle A \rangle_T^2 \tag{2.60}$$

$$\langle \delta A^2 \rangle_T = \langle \delta A(0) \delta A(0) \rangle_T = [\langle A^2 \rangle_T - \langle A \rangle_T^2] \tag{2.61}$$

From eq (2.58) with eq (2.60) and eq (2.61),

$$\langle \delta A(0) \delta A(\tau) \rangle_T = \langle \delta A^2 \rangle_T \exp\left(-\frac{\tau}{\tau_r}\right) \tag{2.62}$$

Now, I consider the suspension of small particles. Neglecting the scattering from solvent molecules, the electric field of the scattered light $E_s(t)$ is the superposition of the scattering from each particle in the scattering volume. Assuming that there are N solutes in the scattering volume now,

$$E_s(t) = \sum_{i=1}^{N} E_i(t) \tag{2.63}$$

where E_i is the scattering from single particle. E_i can be written as

$$E_i(t) = a_i E_0 \exp[i(\boldsymbol{q} \cdot \boldsymbol{r}_i(t) - \omega_0 t)] \tag{2.64}$$

where a_i is the coeficient which contains the factor such as the polarizabilty of particles, the distance to the detector, wave vector of the scattered wave, and so on.

E_0 is the field amplitude of the incident wave, $\boldsymbol{r}_i(t)$ is the position of the center of mass of ith particle, and ω_0 is the angular fewquency. Now, I am concerned only with the relative intensity of light, neglecting the prefactor the intensity of light is written as

$$I = EE^* = |E|^2 \tag{2.65}$$

Thus, the scattering intensity is

$$I_s(t) = E_s(t)E_s^*(t) = \sum_{i,j}^{N} a_i a_j^* E_0^2 \exp[i\boldsymbol{q} \cdot (\boldsymbol{r}_i(t) - \boldsymbol{r}_j(t))] \tag{2.66}$$

The time average of $I_s(t)$ becomes

$$\langle I_s(t)\rangle_T = \left[\langle \sum_{i=1}^{N} |a_i|^2 \rangle_T + \sum_{i\neq j} a_i a_j^* \langle \exp[i\boldsymbol{q} \cdot (\boldsymbol{r}_i(t) - \boldsymbol{r}_j(t))] \rangle_T \right] \tag{2.67}$$

If particles are indentical and independent, the second term on the right-hand side of eq (2.67) vanishes. Thus,

$$\langle I_s(t)\rangle_T = N\langle |a_i|^2\rangle_T E_0^2 \tag{2.68}$$

The time-dependent correlation function of the scattered field $E_s(t)$ is defined as

$$G^{(1)}(\tau) \equiv \langle E_s^*(t)E_s(t+\tau)\rangle_T = \langle E_s^*(0)E_s(\tau)\rangle_T \tag{2.69}$$

Here, because $E_s(t)$ is a stationary random variable and its properties are independent of the time origin, the second identity formula holds. From eq (2.63) and eq (2.64), eq (2.69) is described as

$$G^{(1)}(\tau) = \sum_{i,j=1}^{N} \langle a_i(0)^* a_j(\tau) \exp[i\boldsymbol{q} \cdot (\boldsymbol{r}_i(0) - \boldsymbol{r}_j(\tau))]\rangle_T E_0^2 \exp(-i\omega_0\tau) \tag{2.70}$$

If the defferent particles move independently, and the translational and rotational motions are uncorrelated, eq (2.70) becomes

$$G^{(1)}(\tau) = N\langle a(0)^* a(\tau)\rangle_T \langle \exp[i\boldsymbol{q} \cdot (\boldsymbol{r}(0) - \boldsymbol{r}(\tau))]\rangle_T E_0^2 \exp(-i\omega_0\tau) \tag{2.71}$$

baceuse $a_i(t)$ depends on the orientation of particles due to the polaribility. It is noted that the subscript i is dropped in eq (2.71) for simplicity. In real measurement, we measure the scattered intensity $I_s(t)$ rather than the scattered wave $E_s(t)$. Thus, directly measured quantity is the time-dependent correlation function of $I_s(t)$, which are defined as

$$G^{(2)}(\tau) \equiv \langle I_s(0)I_s(\tau)\rangle_T \tag{2.72}$$

When $E_s(t)$ is a Gaussian random variable, the following relation is held.

$$G^{(2)}(\tau) = \langle I_s(0)^2 \rangle_T + |G^{(1)}(\tau)|^2 \qquad (2.73)$$

This relation is called the Siegert relation, which is important for linking the intensity-intensitr correlation function $G^{(2)}(\tau)$ with the amplitude-amplitude ccorrelation function $G^{(1)}(\tau)$. However, this relation becomes invalid for some systems. For example, in gels or glasses, the movement of scattering elements is limited around their average position. Because in these materials, the important assumption that each particle is independent is no longer valid. It is conventional to define the normalized first and second order correlation function $g^{(1)}(\tau)$ and $g^{(2)}(\tau)$ as

$$g^{(1)}(\tau) \equiv \frac{\langle E_s^*(0)E_s(\tau) \rangle_T}{\langle I_s(0) \rangle_T} = \frac{G^{(1)}(\tau)}{G^{(1)}(0)} \qquad (2.74)$$

$$g^{(2)}(\tau) \equiv \frac{\langle I_s(0)I_s(\tau) \rangle_T}{\langle I_s(0) \rangle_T^2} = \frac{G^{(2)}(\tau)}{|G^{(1)}(0)|^2} \qquad (2.75)$$

Thus, eq (2.73) is written as

$$g^{(2)}(\tau) = 1 + |g^{(1)}(\tau)|^2 \qquad (2.76)$$

For small isotropic scatters, $g^{(1)}(\tau)$ is given as below with substituting eq (2.68) and eq (2.71) into eq (2.74)

$$g^{(1)}(\tau) = \langle \exp[i\boldsymbol{q} \cdot (\boldsymbol{r}(\tau) - \boldsymbol{r}(0))] \rangle_T \exp(-q\omega_0\tau) \qquad (2.77)$$

For translational diffusion, the intermediate scattering $F_s(\boldsymbol{q}, t) = \langle \exp(i\boldsymbol{q} \cdot \boldsymbol{r}) \rangle_T$ can be calculated from using the weighting factor $P(O|\boldsymbol{r}, t)$, which is the conditional probability that a particle will be found in the volume element d^3r at the position $\boldsymbol{r}$ at time t when it were located at the origin initially. Hereafter, $\boldsymbol{r} = \boldsymbol{r}(\tau) - \boldsymbol{r}(0)$ is introduced for simplicity.

$$F_s(\boldsymbol{q}, t) = \int_0^\infty P(O|\boldsymbol{r}, t) \exp(i\boldsymbol{q} \cdot \boldsymbol{r}) d^3r \qquad (2.78)$$

According to Fick's law of diffusion, the particle flux $\boldsymbol{J}$, which is the eate of flow of mass at $\boldsymbol{r}$, is proportional to the gradient of the concentration.

$$\boldsymbol{J}(\boldsymbol{r}, t) = -D_T \nabla c(\boldsymbol{r}, t) \qquad (2.79)$$

The equation of continuity is

$$\frac{\partial c(\boldsymbol{r}, t)}{\partial t} = -\nabla \cdot \boldsymbol{J}(\boldsymbol{r}, t) \qquad (2.80)$$

which assures the conservation of mass. With this equation and eq (2.79), Fick's

secobd law is given as

$$\frac{\partial c(\boldsymbol{r},t)}{\partial t} = D_T \nabla^2 c(\boldsymbol{r},t) \qquad (2.81)$$

In this derivation, it is assumed that D_T is independent of concentration. It is valid only for the limit of low concentration. At low concentration, it can be approximated that $P(O|\boldsymbol{r},t)$ obeys the diffusion equation.

$$\frac{\partial P(O|\boldsymbol{r},t)}{\partial t} = D_T \nabla^2 P(O|\boldsymbol{r},t) \qquad (2.82)$$

The spatial Fourier transform of eq (2.82) gives

$$\int_0^\infty \exp(i\boldsymbol{q}\cdot\boldsymbol{r})\frac{\partial P(O|\boldsymbol{r},t)}{\partial t}d^3r = D_T \int_0^\infty \exp(i\boldsymbol{q}\cdot\boldsymbol{r})\nabla^2 P(O|\boldsymbol{r},t)d^3$$
$$\frac{\partial F_s(\boldsymbol{q},t)}{\partial t} = -D_T q^2 F_s(\boldsymbol{q},t) \qquad (2.83)$$

It is noted that a following property of Fourier transforms is used here.

$$\int_{-\infty}^\infty \exp(iKy)\frac{\partial^n}{\partial y^n}P(y)dy = (-iK)^n \int_{-\infty}^\infty \exp(iKy)P(y)dy \qquad (2.84)$$

From the initial condition $F_s(\boldsymbol{q},0) = 1$, the solution of eq (2.1.3) is

$$F_s(\boldsymbol{q},t) = \exp(-D_T q^2 t) \qquad (2.85)$$

Substituting eq (2.85) into eq (2.77), the desired expression is obtained as

$$g^{(1)}(\tau) = \frac{G^{(1)}(\tau)}{\langle I_s \rangle_T} = \exp(-D_T q^2 \tau)\exp(-i\omega_0\tau) \qquad (2.86)$$

Conbined eq (2.86) with the Siegert equation eq (2.76), the translational diffusion coefficient D_T is obtained from the DLS measurement.

2.2 Elastic properties of gels

The elastic properties of gels are mainly explained by the entropic elasticity of the polymer chains. This section is written based on the books written by Treloar [44] and Rubinstein and Colby [40].

2.2.1 Affine network model

First, I introduce the affine network model, which was proposed by Kuhn. Here, the following assumption is used.

1. The network contains ν chains per unit volume. Chain is defined as the segment of molecule between adjacent cross-linkers.
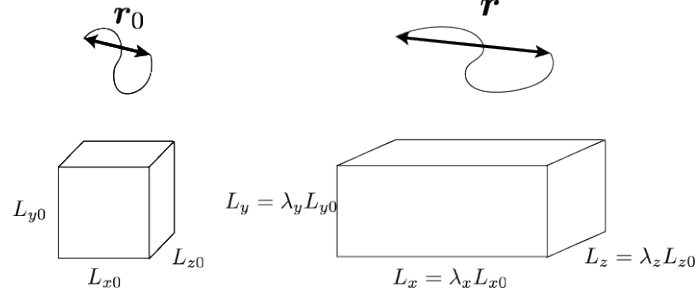2. The mean-square end-to-end distance for the whole assembly of chains in

Figure 2.4: The illustration image of the affine deformation.

the non-deformed state is the same as for a corresponding set of free chains.

3. There is no volume change on the deformation.

4. Each cross-linker moves on the deformation as they were embedded in an elastic continuum. The components of the length of each chain change in the same way with the bulk network. (Affine deformation assumption)

5. The entropy of the network is the sum of the entropies of the individual chains. (Gaussian statistics assumption)

Assumption 4, affine deformation assumption, is the key for the affine network theory because it relates the microscopic deformation of the individual chains to the macroscopic deformation of the material. Here, I consider the deformation shown in Fig. 2.4. In this case, from assumption 3, the following relationship is satisfied.

$$\lambda_x \lambda_y \lambda_z = 1 \tag{2.87}$$

The end-to-end distance of an indivisual chains is represented by the vector $\boldsymbol{r}_0$ with component (r_{x0}, r_{y0}, r_{z0}) in the non-deformed state of the network. After deformation, the component (r_x, r_y, r_z) of the vector length $\boldsymbol{r}$ is described as

$$r_x = \lambda_x r_{x0}, \ r_y = \lambda_y r_{y0}, \ r_z = \lambda_z r_{z0} \tag{2.88}$$

based on assumption 3. The entropy of ideal chains of the non-deformed state $s(N, \boldsymbol{r})$ is described as

$$s(N, \boldsymbol{r}) = -\frac{3k_B \boldsymbol{r}^2}{2Nb^2} + S(N, \boldsymbol{0}) \tag{2.89}$$

where N is the number of segments per chain, b is the segment length, and k_B is the Boltzmann constant. Thus, the contribution of the total entropy of deformation for

the network due to this chain is

$$
\begin{aligned}
\Delta s = s(N, \boldsymbol{r}) - s(N, \boldsymbol{r}_0) &= -\frac{3k_B(\boldsymbol{r}^2 - \boldsymbol{r}_0^2)}{2Nb^2} \\
&= -\frac{3k_B}{2Nb^2}[\{(\lambda_x r_{x0})^2 + (\lambda_y r_{y0})^2 + (\lambda_z r_{z0})^2\} - (r_{x0}^2 + r_{y0}^2 + r_{x0}^2)] \quad (2.90)\\
&= -\frac{3k_B}{2Nb^2}\{(\lambda_x^2 - 1)r_{x0}^2 + (\lambda_y^2 - 1)r_{y0}^2 + (\lambda_z^2 - 1)r_{z0}^2\}
\end{aligned}
$$

The total entropy for all the ν chains contained in unit volume of the network is obtained by the summation of eq (2.90). Assuming that chain countor length and the molecular weight are the same for all chains in the network, the total entropy of deformaton of the network is described as

$$
\Delta S = \sum \Delta s = -\frac{3k_B}{2Nb^2}\{(\lambda_x^2 - 1)\sum r_{x0}^2 + (\lambda_y^2 - 1)\sum r_{y0}^2 + (\lambda_z^2 - 1)\sum r_{z0}^2\} \quad (2.91)
$$

where $\sum$ is the summation for the assembly of ν chains. When the network is the non-deformed state, the directions of the chain vector $\boldsymbol{r}_0$ are entirely random, and there is no preference for the x, y, or z directions. Therefore, considering the assembly of ν chains,

$$
\sum r_{x0}^2 = \sum r_{y0}^2 = \sum r_{z0}^2 = \frac{1}{3}\sum r_0^2 = \frac{1}{3}\bar{r}_0^2 \quad (2.92)
$$

There,

$$
\sum r_{x0}^2 + \sum r_{y0}^2 + \sum r_{z0}^2 = \sum r_0^2 \quad (2.93)
$$

where $\bar{r}_0^2$ is the mean-square length of the chains in the non-deformed state, which are represented as $b^2 N$. Hence, eq (2.91) is written as

$$
\Delta S = -\frac{1}{2}\nu k_B(\lambda_x^2 + \lambda_y^2 + \lambda_z^2 - 3) \quad (2.94)
$$

The Helmholtz free energy change from the deformation, or work of the deformation, ΔW is obtained from the relationship of the thermodynamics $\Delta U = T\Delta S + \Delta W$. In the case for the ideal chains, there is no change of internal energy on deformation ($\Delta U = 0$). Then,

$$
\Delta W = -T\Delta S = -\frac{1}{2}\nu k_B T(\lambda_x^2 + \lambda_y^2 + \lambda_z^2 - 3) \quad (2.95)
$$

where T is the absolute temperature. With eq (2.87) defining that $\lambda_x = \lambda$ is the deformation axis and $\lambda_y = \lambda_z$, eq (2.95) is rewritten as

$$
\Delta W = -T\Delta S = -\frac{1}{2}\nu k_B T(\lambda^2 + 2\lambda^{-1} - 3) \quad (2.96)
$$

The stress σ can be obtained from

$$
\sigma = \partial \Delta W/\partial \lambda = \nu k_B T(\lambda - \lambda^{-2}) \quad (2.97)
$$

where $\nu k_B T$ equals to the shear modulus G'. The relationship of eq (2.97) is called the Neo-Hookean model.

2.2.2 Phantom network model

In the affine network model introduced in the previous section, the main assumptions are assumptions 4 and 5: the ends of chains (the cross-linkers junction) are fixed in space and are deformed affinely with the bulk network as if they were permanently attached to some elastic background. However, in real networks, each chain is connected to other chains at cross-linkers, and these cross-linkers are not fixed in space. The cross-linkers fluctuate around their average positions, which leads to a net lowering of the free energy of the system by reducing the cumulative stretching of the network. The phantom network model was proposed by James and Guth to consider these fluctuation effects. Here, each ideal chain obeys Gaussian statistics with ends joined as cross-linkers. From mathematical analysis, it is revealed that the fluctuation of any junction point in the network of Gaussian chains may be described by the Gaussian probability function. The mean value of the fluctuations of any given junction point is independent of the strain in the bulk network. The non-fluctuation junction is only the junctions at the surface of the network, and these junctions are attached to the elastic non-fluctuating boundary of the network. This attachment fixes the volume of the phantom network and prevents its collapse which would occur the excluded volume interaction between monomers is ignored in such simple models.

From Gaussian statistical treatment, it is led that the fluctuation of a single monomer in an ideal chain with fixed ends is identical to the fluctuation of an end monomer of a single effective chain of K monomers. For example, the fluctuation of the center monomer of an ideal chain with $2N$ monomers is identical to that of an end of the effective chain which has $K = N/2$ monomers. Thus, the constraining effect of the two strands of N monomers is identical to the constraining effect of a single effective chain of $K = N/2$ monomers.

I consider an f-arm star polymer with molecular weight N of an arm (Fig. 2.5). The fluctuation of junction points in a network is regarded as those of the branch point of an f-arm star polymer. Here, $f - 1$ arms are attached at one end to the surface of the network and joined at the other end by a junction point, which connects these $f - 1$ arms to a single arm. The chains attached to the elastic non-fluctuating network surface are called seniority-zero chains. The seniority of a particular chain is defined by the number of other chains along the shortest path between its chain and the network surface. A single seniority-one chains is connected to $f-1$ seniority-zero chains at the f functional junction point. These $f-1$ seniority-zero chains can be replaced by a single effective chain containing K_1 monomers with
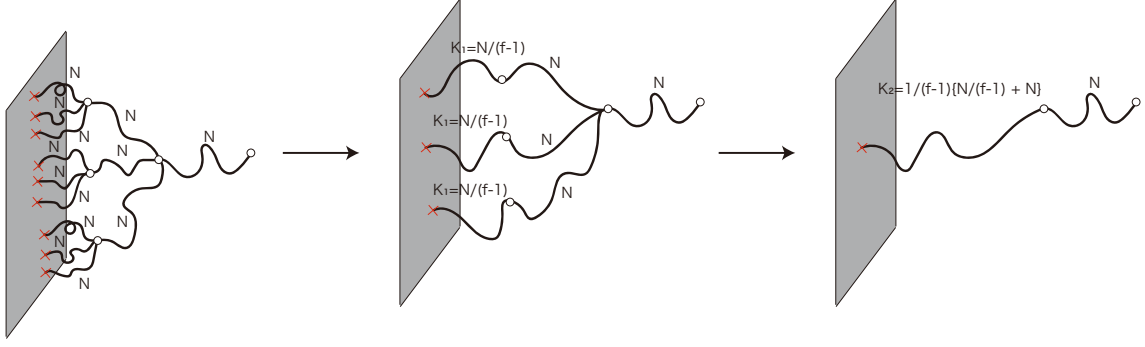
Figure 2.5: Recurrence relation diagrams for the effective chains of the phantom network model from the each ideal chains ($f = 4$).

the same constraining effect as the $f - 1$ original chains:

$$K_1 = \frac{N}{f - 1} \tag{2.98}$$

This single effective chain is then adjacent to a single seniority-one with N monomers. $f - 1$ effective chain of $K_1 + N$ monomers is further connected to the junction point of functionality f. Thus, $f - 1$ these seniority-zero and seniority-one chains can be also replaced by one effective chain:

$$K_2 = \frac{1}{f - 1}(K_1 + N) = \frac{1}{f - 1}\left(\frac{N}{f - 1} + N\right) \tag{2.99}$$

This effective chain is connected to the seniority-two chain. Thus, constraining effect combined from seniority-zero chains though seniority-two chain is discribed as

$$K_2 + N = \frac{1}{f - 1}\left(\frac{N}{f - 1} + N\right) + N = N\left\{1 + \frac{1}{f - 1} + \left(\frac{1}{f - 1}\right)^2\right\} \tag{2.100}$$

Continuing this procedure from seniority-zero chains though an arbitrarily large seniority. This procedire gives a geometric series, which this series rapidly converges. Each junction point in the bulk of a phantom network can be regarded as connected to the elastic non-fluctuating surface of the neteork though f effective chains with K monomers in each.

$$K = N\left\{1 + \frac{1}{f - 1} + \left(\frac{1}{f - 1}\right)^2 + \left(\frac{1}{f - 1}\right)^3 + ...\right\}$$
$$= \frac{N}{1 - 1/(f - 1)} = \frac{f - 1}{f - 2}N \tag{2.101}$$

To calculate the shear modulus of the phantom network, it is necessary to consider the fluctuation of chains between two adjacent junction points. In this condition, each junction point is attached to the elastic non-fluctuating surface with $f - 1$ effective chains of K monomers. These $f - 1$ effective chains can be replaced by a

single effective chain of $K/(f-1)$ monomers further. Finally, the chain between two adjacent junction points is described as one combined chain of N_p monomers:

$$N_p = \frac{2K}{f-1} + N = \frac{f}{f-2}N \qquad (2.102)$$

From eq (2.90), (2.91), and (2.96) , the free energy change due to defromation in the phantom network is

$$\Delta W = \frac{f-2}{f}\frac{3k_BT\Delta r^2}{2Nb^2} \qquad (2.103)$$

Therefore, the shear modulus G' is led with same procedure with the affine netwrok model,

$$G = \nu K_B T \frac{f-2}{f} \qquad (2.104)$$

For any functionality f, the phantom network model predicts the lower G' compared with the affine network model due to the fluctuation of junction points. The density of chains of the network is the same between the affine and phantom network, however, in the phantom network, the fraction $(f-2)/f$ of the combined chain is the real elastic chain that supports stress. For the perfect network with no defects, the phantom network modulus G' is proportional to the difference of the number densities of network elastic chains ν and cross-linkers $\mu = 2\nu/f$ because there are $f/2$ network elastic chains per cross-linkers.

$$G' = (\nu - \mu)k_B T \qquad (2.105)$$

2.2.3 Tree-like approximation

To predict the shear modulus G' based on the affine or phantom models, the number density of network elastic chains ν and cross-linkers μ are essential. These parameters are not predicted from the preparation condition directly and an approximation model is necessary. Here, I introduce the tree-like approximation by Miller and Macosko [45] for prediction of ν and μ. In this model, the following assumptions are retained.

1. All functional groups of the same type polymers have equal reactivity.
2. All groups react independently of one another.
3. The intramolecular reactions do not occur in finite species.

For simplicity, I consider the reaction of tetra-arm tetra-functional polymers. Gelation reaction proceeds until the fraction p of the termination of the polymer
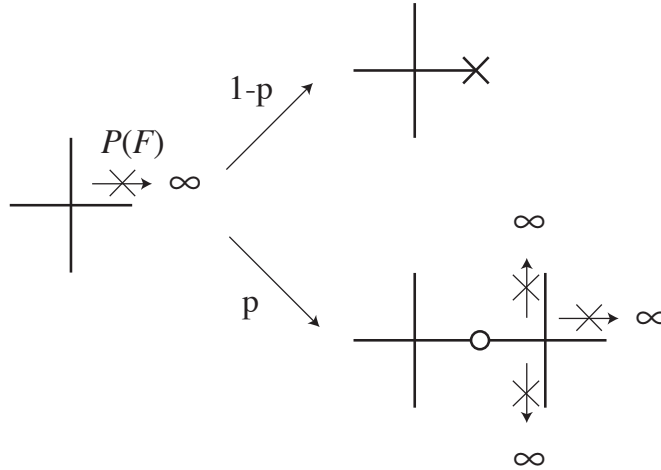
Figure 2.6: Schematic image of the process of a reaction of the tetra-arm polymer.

has reacted, which is the identification of reaction efficiency of gels. In this model, the probability of a complimentary event that tetra-arm polymer connects to the infinite network, $P(F)$, is considered. As shown in Fig. 2.6, there are two cases about the reaction of tetra-arm polymer. One is the case of the reaction terminated without any reaction with any other polymers $(1 - p)$. This case is just summed for $P(F)$. The other case is that the tetra-arm polymer reacts with another tetra-arm polymer. In this case, when the other three arms do not react to any other polymers, this results in not connecting the infinite network. Thus, the probability to lead the finite network through this route is $p \cdot P(F)^3$. Eventually,

$$P(F) = p \cdot P(F)^3 + (1 - p) \tag{2.106}$$

This equation can be transformed as

$$(P(F) - 1)(p \cdot P(F)^2 + p \cdot P(F) + p - 1) = 0 \tag{2.107}$$

The solution of eq (2.107) is

$$P(F) = \sqrt{\frac{1}{p} - \frac{3}{4}} - \frac{1}{2} \tag{2.108}$$

in the range $0 \leq P(F) \leq 1$ excepted for the solution of $P(F) = 1$. When three arms or tetra arms of tetra-arm polymers connect to the infinite network, these polymers become the junction point. The probability that tetra-arm polymer beocmes f functional junction point is

$$P(X_3) = {}_4C_3 P(F)(1 - P(F))^3 \tag{2.109}$$

$$P(X_3) = {}_4C_4 (1 - P(F))^4 \tag{2.110}$$

Thus, the number density of cross-linkers μ_0 and the network elastic chains ν_0 is

$$\mu_0 = \Phi \left(P(X_3) + P(X_4) \right) \tag{2.111}$$

$$\nu_0 = \Phi \left(\frac{3}{2} P(X_3) + \frac{4}{2} P(X_4) \right) \tag{2.112}$$

where Φ is the number density of the tetra-arm polymers. It should be noted that ν_0 is devided by 2 to prevent double count.

CHAPTER 3

Examination of origin of spatial heterogeneity and quantification of spatial heterogeneity

3.1 Introduction

As described in chapter 1, the "bond percolation" concept provides the highly homogeneous gel by presenting a simple yet universal scheme, which has disproved the preconception that gels are inherently spatial heterogeneous [39]. In the previous study, bond percolation conditions were easily achieved by crosslinking tetra-functional star polymers (Fig. 3.1(A)) with small bi-functional cross-linkers (Fig. 3.1(B)) at a sufficiently high polymer concentration in a solvent with high affinity toward the polymer units (Fig. 3.1(C), (F)). The use of a high polymer concentration ensures that the polymer units fill the entire solution space, and the use of a high-affinity solvent prevents the potential aggregation of polymer chains during the gelation process. The homogeneity of the developed gel was investigated in the Fourier space using light and X-ray scattering techniques, as well as mechanical tests. The gel network formed under the bond percolation condition was highly spatial homogeneous; neither static laser speckles nor anomalous small-angle scattering was observed, and the obtained gels exhibited fully ergodic concentration fluctuations and ideal rubber elasticity. These properties completely contradicted the then widely accepted picture of gels [26, 35, 46–53].

In this chapter, I further develop this strategy of controlling the percolation process and demonstrate that in addition to removing the typical spatial defects present in gels, it is possible to selectively induce predefined spatial defects into the gel network by tuning the initial packing conditions in the pre-gel solutions. I used the same star polymer units and the same crosslinking chemistry (Fig. 3.1(A), (B)), but changed the packing fraction of star polymers in the pre-gel solution and tuned the affinity between the polymer chains and the solvent. Under the low-packing-fraction condition, the pre-gel solution is only partially filled with star polymer units (Fig.

3.1(D)), and the formation of the gel network is dominated by the diffusion of the polymer units [54]. This condition is known as "site percolation" [55]. The formed gel network is expected to contain microscopic voids where the local polymer concentration is almost zero (Fig. 3.1(G)). In contrast, under the low-affinity condition, polymer-rich aggregates are formed in the pre-gel solution [56] and further develop during the gelation process (Fig. 3.1(E)). Although the polymer concentration is high enough for the polymer units to fill the solution space uniformly, some chains localize to occupy the same site due to low polymer-solvent affinity. This breaks the ideal bond percolation condition and resulted in gel networks with locally concentrated regions (Fig. 3.1(H)). Hereafter, I refer to gels formed at the ideal condition as "bond percolation gels" (Fig. 3.1(F)), to those at low packing ratio as "site percolation gels" (Fig. 3.1(G)) and to those at high packing ratio but with aggregates in the pre-gel solution as "non-ideal bond percolation gels" (Fig. 3.1(H)). The voids and aggregates will similarly disturb the passage of light through gels because both negative and positive deviation of local polymer concentrations results in the same extent of light scattering. However, as for the mechanical properties, while the aggregates lower the elastic modulus according to the number of polymers do not join the gel network, the voids may cause a significant decrease of elastic modulus because of the additional topological defects by the insufficient chain packing [57,58]. Although gel structures have been widely studied for decades, the selective addition of predefined defects has not been achieved yet. The controlled introduction of such defects may effectively modulate the mechanical, optical, and mass-transportation properties of the gels. Moreover, the success of the selective doping of the defects indicates the effectiveness of the bond percolation concept for the fabrication of spatial homogeneous gels.

3.2 Experimental section

3.2.1 Sample preparation

poly(ethylene glycol) terminated with N-hydroxysuccinimidyl ester (tetra-PEG-NHS; M_w= 20 kg/mol) was purchased from SINOPEG (Xiamen, China), and 1,14-diamino-3,6,9,12-tetraoxatetradecane (amino-PEG4-amine) was purchased from Sigma-Ardrich (St. Louis, USA). All other chamicals were purchased from Fujifilm Wako Pure Chemical Corp. (Osaka, Japan). All gel samples were synthesized by cross-linking tetra-PEG-NHS (Fig. 3.1(A)) with the small cross-linker, i.e., amino-PEG4-amine (Fig. 3.1(B)). A molar concentration of amino-PEG4-amine was twice that of tetra-PEG-NHS was used in order to achieve equal molar concentrations of amine and NHS groups. The details of the different gel samples are as follows. (1) The bond percolation gel was synthesized using a high concentration (c = 6 mM >
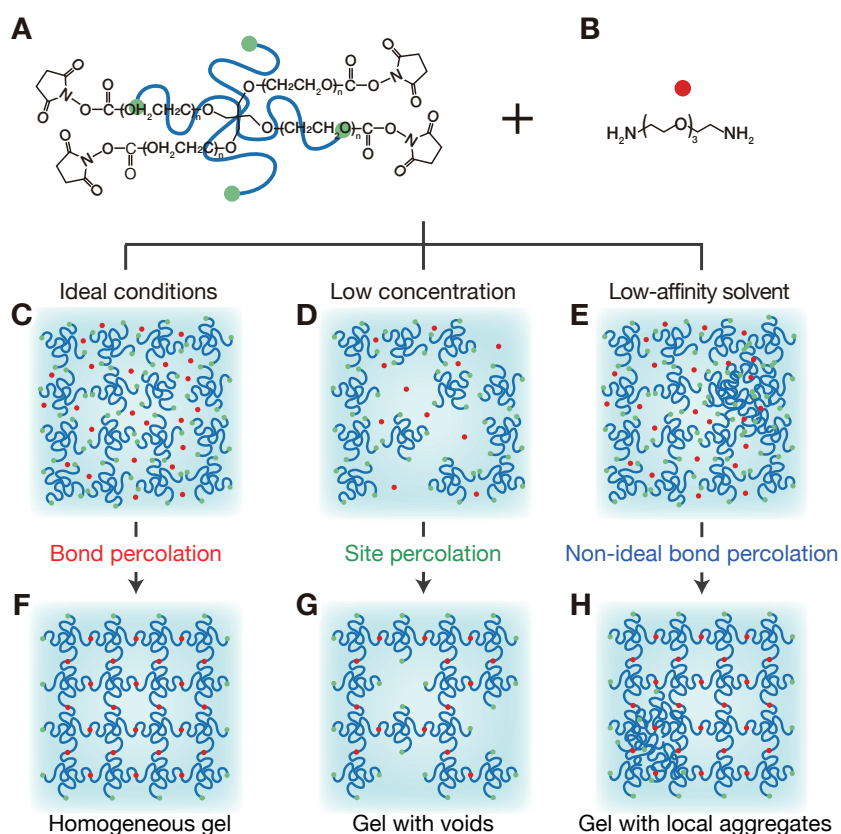
Figure 3.1: Illustration of the scheme used to prepare gels with different types of spatial heterogeneity. All the gels were synthesized by crosslinking (A) star polymer units that consist of tetrafunctional poly(ethylene glycol) (PEG) with active ester end groups with (B) the bifunctional cross-linker 1,14-diamino-3,6,9,12-tetraoxatetradecane (amino-PEG4-amine). (C-E) Three different geometrically constrained conditions were applied to the pre-gel solutions in order to induce different percolation processes. (F-H) Expected structures of the resulting gel networks.

c^*) in dehydrated acetonitrile, which is a good solvent for the PEG chains, containing 100 mM acetic acid (Fig. 3.1(C), (F)). c^* is the concentration at which chain overlap of tetra-PEG-NHS ($c^* \approx 3$ mM) occurs, which was estimated using light-scattering measurements (Fig. 3.2). (2) The site percolation gel was synthesized in the good solvent, i.e., acetonitrile containing 30 mM acetic acid, but at a low polymer molar concentration (c = 1.5 mM < c^*) (Fig. ??D, G). (3) The non-ideal bond percolation gel was synthesized using a high polymer concentration ($c = 6$ mM > c^*) in an aqueous sodium phosphate buffer containing NaH_2PO_4 and Na_2HPO_4 (total concentration 100 mM; pH = 6.6), which shows lower affinity toward PEG chains than acetonitrile [35, 37, 59] (Fig. ??(E), (H)). All the pre-gel solutions were filtered through 0.2 μm PTFE syringe filters (ADVANTEC Toyo Co. Japan) before being mixed with the crosslinkers. Acetic acid or sodium phosphates were added
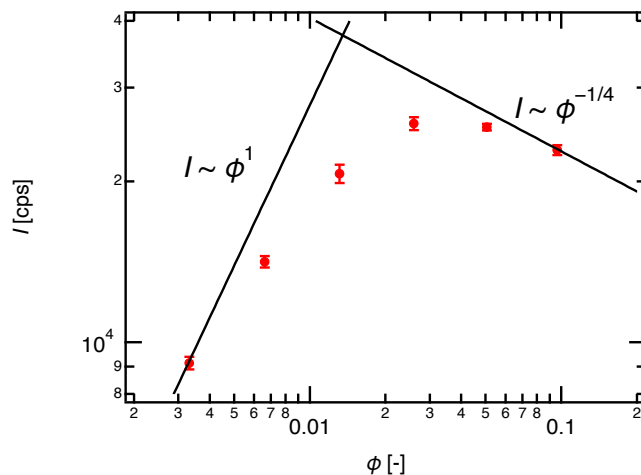
Figure 3.2: Scattering intensity I of tetra-PEG-NHS in acetonitrile for various polymer concentrations (c = 0.188, 0.375, 0.75, 1.5, 3, and 6 mM) as a function of ϕ. The scattered intensity from each solution was measured for 300 s at a scattering angle of 90° using a He-Ne laser (λ = 632.8 nm). The solvent scattering was subtracted. The solid lines are guides representing the theoretical scaling relations for a dilute ($I \sim \phi^1$) and semidilute solution ($I \sim \phi^{-1/4}$) in a good solvent, respectively.
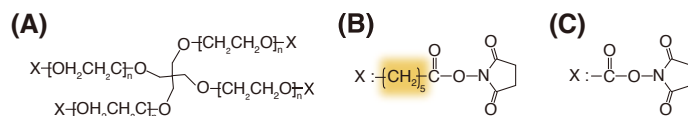

Figure 3.3: Difference between the chemical structure of the tetra-PEG used in the previous study and the present study [39]. (A) General structure of tetra-PEG. (B) PEG end group in the previous study. The alkyl chain indicated by the orange box was not present in this study. (C) PEG end group used in this study.

to the solvents to tune the rate of reaction between the NHS and amine groups. It should be noted that the gelation time (t_{gel}) of the bond percolation gel synthesized in this study ($t_{\text{gel}} \approx 10$ min) was faster than that in the previous study [39] ($t_{\text{gel}} \approx 60$ min) although the same amount of acetic acid was added. The different t_{gel} resulted from the different chemical structure near the end-groups in the tetra-PEG-NHS used in this study compared to the previous study (Fig. 3.3).

3.2.2 Dynamic mechanical analysis

The dynamic mechanical analysis of each gelation process was conducted using a rheometer (MCR501, Anton Paar, Austria). I used a concentric cylinder geometry with a cup of 18.00 mm in diameter and a rotation jig of 16.65 mm in diameter.

The solutions of amino-PEG4-amine and tetra-PEG-NHS were mixed for 30 sec and then gently poured into the cup of the rheometer. The air bubbles in the cup were carefully removed before starting the measurement. After the sol-gel transition occurred, a small amount of paraffin oil was gently putted on the top of gel samples to avoid the evaporation of the solvent during the real-time measurements. The shear strain, shear frequency, and temperature were 2%, 1 Hz and 25 $°C$, respectively. Linear viscoelasticity properties were confirmed at this shear strain.

3.2.3 2D Laser speckle imaging
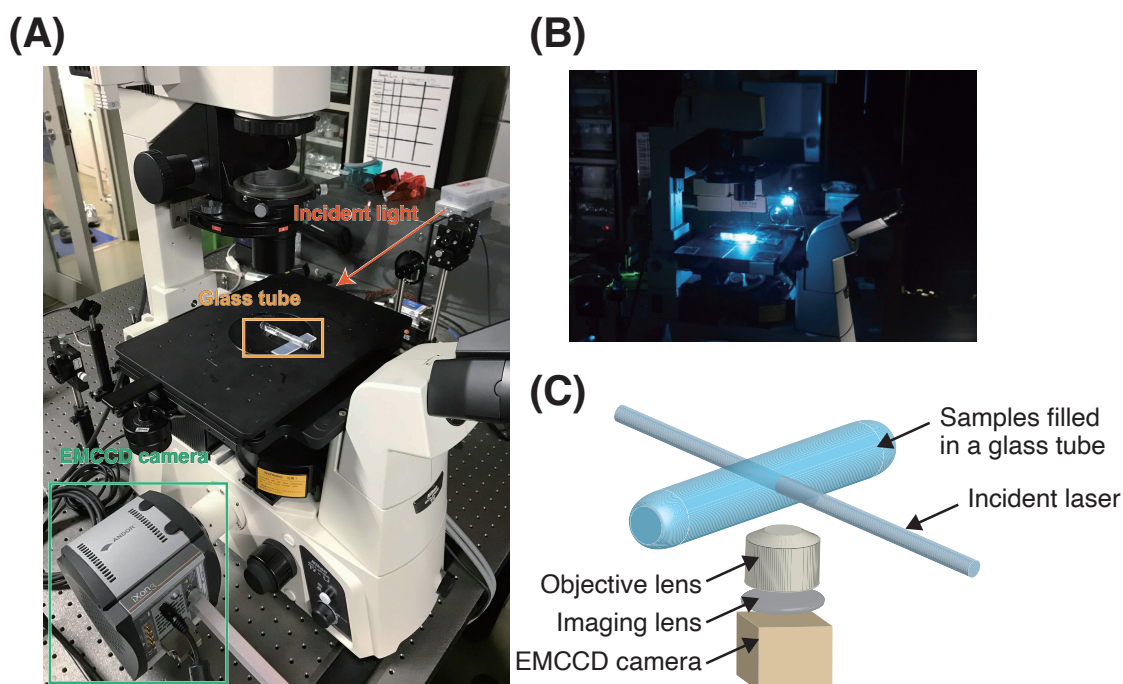
Figure 3.4: (A) A photograph of the measurement setup of 2D Laser speckle imaging. (B) A photograph of the measurement setup when samples was irradiated laser. (C) An illustration of the measurement setup.

2D Laser speckle imaging was carried out using an inverted microscope (ECLIPSE Ti-U, Nikon, Japan). Gel samples were synthesized in glass tubes (diameter: 8 mm), which were placed on the stage of the microscope. A coherent laser beam (λ = 473 nm; coherent length: 100 m; beam diameter: 0.7 mm; Cobolt Blues, Cobolt, Sweden) was directed onto the glass tube parallel to the microscope stage. The scattered light was collected via a 10 × objective lens (TU Plan Fluor EPI, Nikon, Japan) and recorded using an electron multiplying charge-coupled device (EMCCD) camera (iXon3, Andor Technology, England). Measurements were conducted at ambient temperature ($\sim$25 °C). A photograph and an illustration of measurement

setup is shown in Fig. 3.4.

3.2.4   1D Static light scattering

1D Static light scattering (SLS) measurements were carried out on the gel samples using a commercial light-scattering instrument (ALV-5000, ALV, Germany) with a He-Ne laser (λ = 632.8 nm) as the incident light source. Gel samples for the SLS experiments were synthesized in glass tubes (diameter: 8 mm). The scattered light was collected at scattering angles between 30° to 150° with three times of 10 s exposures at each angle. To obtain the ensemble-averaged scattering intensity, the samples were continuously rotated during the measurements using an automatic sample-rotation stage. Toluene was used as a standard to scale the raw scattering intensity to the excess Rayleigh ratio. The excess Rayleigh ratio was then scaled to match the absolute intensity of the small-angle X-ray scattering (SAXS). All measurements were conducted at 25 °C.

3.2.5   Small-angle X-ray scattering(SAXS)

SAXS measurements were carried out at the BL-6A beam line of the Photon Factory, High Energy Accelerator Research Organization, KEK (Ibaraki, Japan). The wavelength of the incident X-rays was 0.15 nm, and the beam diameter at the sample position was approximately 0.25×0.50 mm^2. The exposure time per sample was 30 s, and the sample-to-detector distance was 2.54 m. The scattering profile was collected using a 2D hybrid pixel detector (PILATUS3 1M, DECTRIS Ltd., Switzerland). All measurements were conducted at ambient temperature ($\sim$25 °C). The gel sample (thickness: 1 mm) was contained in a custom-made planar cell and sealed with two 30 μm thick glass windows. The scattered intensity was circularly averaged to obtain the 1D intensity profile and then corrected for incident beam flux, sample absorption and thickness, as well as exposure time and cell and solvent scattering using a custom-made data reduction package Red2D (https://github.com/hurxl/Red2D) within a scientific data analysis software package (Igor Pro 8, WaveMetrics). The intensity was plotted as a function of the magnitude of the scattering vector, q. Glassy carbon (National Institute of Standards and Technology (NIST), USA) and silver behenate (Nagara Science, Japan) standards were used for calibration. The $I(q)$ values of the SAXS profile of the non-ideal bond percolation gel were scaled by a factor of 10.9, which is the theoretical ratio between the contrast of PEG-acetonitrile and PEG-water estimated using the NIST scattering length density (SLD) calculator (https://www.ncnr.nist.gov/resources/activation/) (for details of the calculations, see the Supporting Information).

3.2.6 Dynamic light scattering

Dynamic light scattering (DLS) experiments were carried out on the gel samples using the same light-scattering instrument as for the SLS experiments. The scattering angle was fixed at 90°. All the samples were measured at 100 different, randomly chosen positions for 30 s per position using an automatic rotation and vertical motion unit. All measurements were performed at 25 °C.
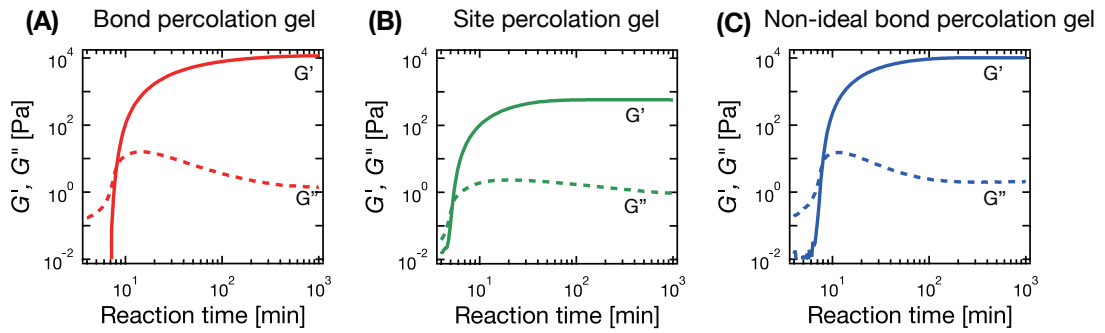
3.3 Results and Discussion

Figure 3.5: Shear-storage modulus (G') and shear-loss modulus (G'') during the gelation processes of the (A) bond percolation gel, (B) site percolation gel, and (C) non-ideal bond percolation gel.

First, I confirmed the gelation of each gel using dynamic mechanical analysis (Fig. 3.5). Under all percolation conditions, the shear-storage moduli (G') overtook the shear-loss moduli (G'') during the gelation process, indicating the successful formation of a gel network. The percolation point, or gel point (t_{gel}), for each condition was determined as the crossover point of G' and G'' [60]. The t_{gel} of each gel was tuned in the range of 5-10 min by adding base or acid to the pre-gel solution. The values of G' reached a plateau within 1000 min, indicating the completion of the network formation. While the final G' value of the bond percolation (Fig. 3.5(A)) was as high as ~12 kPa, it decreased to ~600 Pa for the site percolation gel (Fig. 3.5(B)) and ~10 kPa for the non-ideal bond percolation gel (Fig. 3.5(C)). By applying a rubber elasticity model (the phantom network model) [61] with a tree-like approximation [45] to the final values of G', the crosslinking ratios between the star polymer units can be estimated. In the phantom network model, G' is described as

$$G' = (\nu - \mu)k_{\mathrm{B}}T \tag{3.1}$$

where ν and μ are the number density of elastically effective chains and the number density of branch points, respectively. k_{B} is the Boltzmann constant, and T is the absolute temperature. With a tree-like approximation, $\nu - \mu$ for the case of

cross-linking of 4-arm star polymer with small cross-linkers can be estimated as

$$\nu - \mu = u_4 \left\{ 2 \cdot \left[\left(\frac{1}{P} - \frac{3}{4} \right)^{1/2} - \frac{1}{2} \right] \cdot \left[\frac{3}{2} - \left(\frac{1}{P} - \frac{3}{4} \right)^{1/2} \right]^3 + \left[\frac{3}{2} - \left(\frac{1}{P} - \frac{3}{4} \right)^{1/2} \right]^4 \right\}$$
(3.2)

where u_4 is the number density of tetra-PEG-NHS in the gel and P is the cross-linking ratio, which is given by:

$$P = p^2 \tag{3.3}$$

where p is the reaction conversion of the terminating groups of tetrafunctional PEG [62]. The estimated values were 90%, 55%, and 85% for the bond percolation, site percolation, and non-ideal bond percolation gels, respectively. Here, the crosslinking ratio is defined as the number fraction of star polymer arms that are connected to another arm. The low crosslinking ratios in the site percolation and non-ideal bond percolation gels indicated the presence of elastic defects, such as dangling ends, loops and unfavorable crosslinking. The significant increase of the elastic defects has been confirmed when the initial packing ratio is low [57, 63].
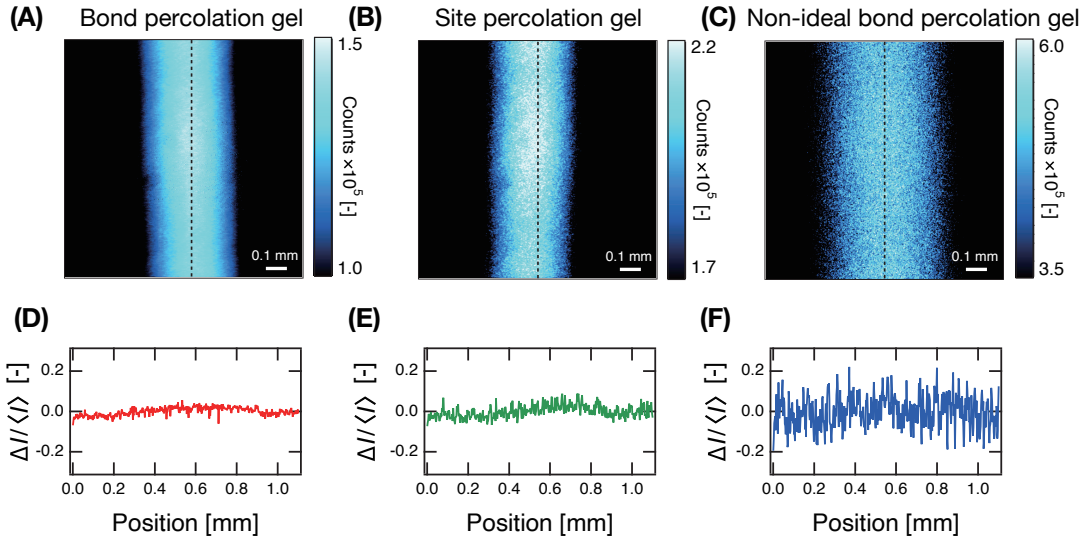
Figure 3.6: (A-C) 2D Static laser speckle images from the corresponding fully developed gels. Each laser speckle image was accumulated for 30 s. (D-F) Corresponding plot of the deviation of the intensity from the mean ($\Delta I / \langle I \rangle$) vs pixels. The positions of the pixels are indicated by the vertical dashed line in panels A-C.

The presence of the spatial defects in the gels was visually confirmed using 2D laser-light speckle tests (Fig. 3.6(A-F)). All images were recorded for 30 s to obtain time-averaged static laser speckle patterns. Static laser speckles, i.e., bright spots, which indicate time-independent spatial heterogeneities [50, 64–67], were not
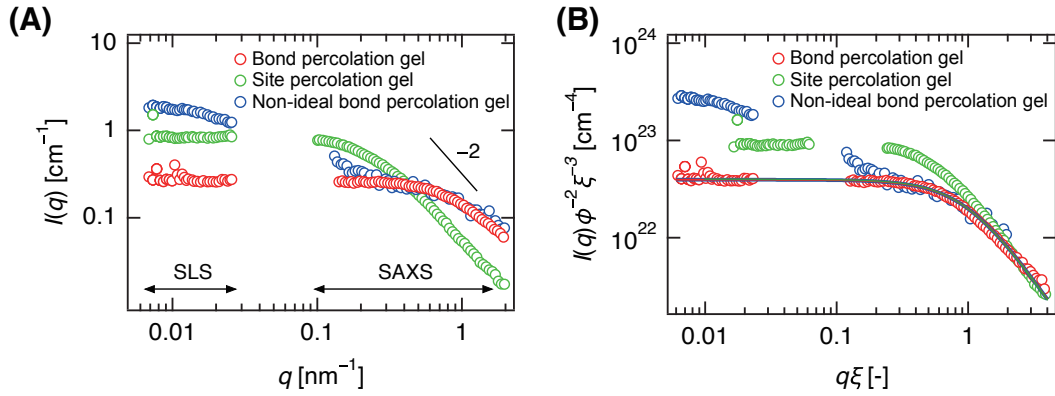
Figure 3.7: Nanostructure of the fully developed gels synthesized under different percolation conditions. (A) Scattering profiles shown at absolute scale after scaling $I(q)$ to correct for differences in scattering contrast, i.e., the difference in scattering length density ($\Delta\rho$) and refractive index increment, using the $\Delta\rho$ value of PEG/ACN as a reference (Fig. 3.8). The solid line is a guide depicting the scaling relation $I(q) \sim q^{-2}$. (B) Scattering profiles normalized with respect to the contribution of thermodynamic fluctuations in terms of ξ and ϕ. The red and blue solid curves are the fittings with the Ornstein Zernike (OZ) model (eq (3.4)) for the bond percolation and non-ideal bond percolation gel, respectively. The green solid curve shows the theoretical OZ curve for the site percolation gel estimated using the theoretical scaling ($\xi \sim \phi^{-3/4}$) and the values of the bond percolation gel. All three curves overlap for $q\xi \geqq 1$.

observed in the bond percolation gel (Fig. 3.6(A)), suggesting high spatial homogeneity. In contrast, numerous laser speckles were observed in the site percolation (Fig. 3.6(B)) and non-ideal bond percolation gels (Fig. 3.6(C)), indicating that these gel networks contain spatial defects. It should be noted that the scattering intensity of gels is correlated with a total polymer volume fraction and a presence of static heterogeneities, which leads to the difference of the scattered intensity for each sample (Fig. 3.6(A-C)). The deviation of the local scattering intensity from the averaged scattering intensity $\Delta I/\langle I \rangle$ is shown in Fig. 3.6(D-F) to signify the presence of speckles as effects of the scattered intensity are eliminated. Fluctuations of the scattered intensity of both the site percolation gel and the non-ideal bond percolation gel from the average are larger than the bond percolation gel. These fluctuations mean a speckle pattern. The speckle pattern of the non-ideal bond percolation gel was much more vivid than that of the site percolation gel, suggesting that the size and/or number of defects in the former gel is higher than in the latter [41, 43].

To quantitatively characterize the spatial defects, I performed static light scattering (SLS) and small-angle X-ray scattering (SAXS) measurements to estimate the size and the volume fraction of the defects (Fig. 3.7(A)). In the bond percolation gel, a transition shoulder from a plateau in the low-q region to a power-law-type
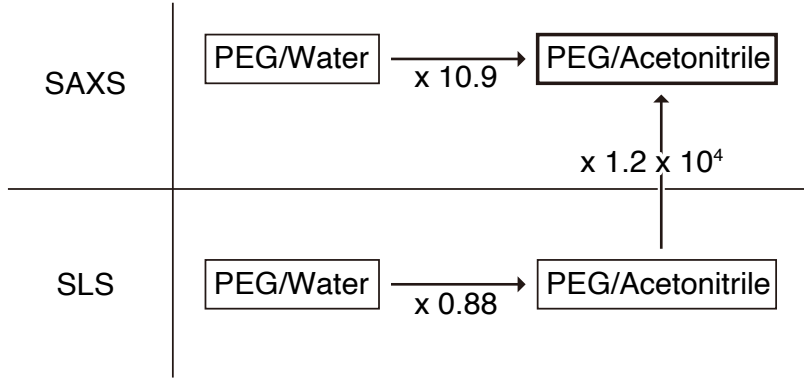
Figure 3.8: Diagram of the different scattering contrasts in PEG/water and PEG/Acetonitrile systems measured using SLS and SAXS. All scattering profiles were scaled based on this diagram using the SAXS profile of PEG/Acetonitrile as a reference. Details of the scaling factors are given in the above section.
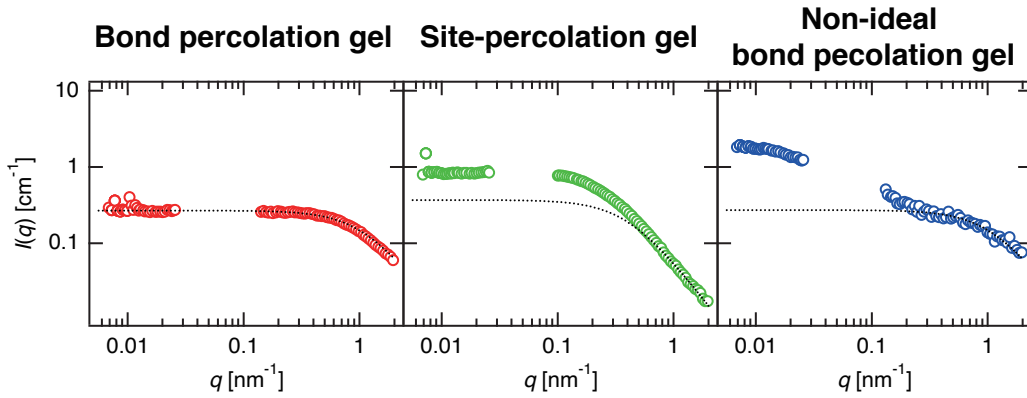
Figure 3.9: Fitting curves (homogeneous gel and non-ideal bond percolation gel) using the Ornstein-Zernike model and the theoretical curve (site percolation gel) estimated from the fitting parameters obtained from the homogeneous gel using the scaling relation $\xi \sim \phi^{-3/4}$ and eq (3.4). Details of the calculation of the theoretical curve are described above in this document. The profile of $I(q)$ has been vertically scaled using $\Delta\rho$ of PEG/Acetonitrile as a reference as described above.

decay in the high-q region was observed at $q \approx 1$ nm^{-1}. This type of $I(q)$ profile is commonly observed for semidilute polymer solutions and gels, and reflects the thermodynamic fluctuations of the crowded polymer chains [68, 69]. The value of $I(q)$ at $q \to 0$, $I(0)$, is related to the isothermal osmotic compressibility of the system. The transition point of $I(q)$ denotes the screening length of the excluded volume effect between the segments in the polymer chains, or simply the size of a correlation blob (ξ) [40, 70, 71]. These thermodynamic parameters can be estimated by fitting $I(q)$ using the Ornstein-Zernike (OZ) model [71], which is a scattering model for the
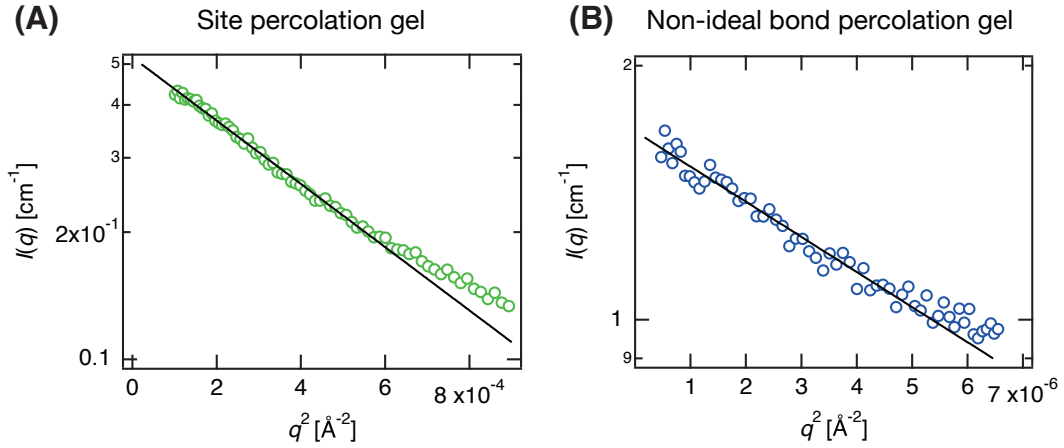
Figure 3.10: Guinier plot of (A) the site percolation gel and (B) the Non-ideal bond percolation gel. The contribution from thermodynamic fluctuations was subtracted in the graph shown above. The solid line is the fitting curve obtained using eq (3.5)

thermodynamic fluctuations in uniform systems:

$$I(q) = \frac{I_{OZ}(q)}{1 + \xi^2 q^2} \tag{3.4}$$

where $I_{OZ}(0)$ is the scattering intensity at $q = 0$, which is proportional to $\phi^2 \xi^3$. The model fitted well for the bond percolation gel data as shown in Fig. 3.9; the fitting parameters are listed in Table 3.1. ξ was estimated to be 0.9 nm, which is much smaller than the radius of gyration (R_g) of the star polymer unit in the pre-gel solution ($R_g \approx 3.5$ nm for tetra-PEG-NHS with $M_w = 20$ kg/mol) [35], confirming that the shoulder in the plot of $I(q)$ originates from the thermodynamic fluctuations of crowded polymer chains in the solvent.

The $I(q)$ profile of the non-ideal bond percolation gel overlapped well with that of the bond percolation in the high-q region ($q > 0.3$ nm^{-1}), which covered the length scale of the thermodynamic fluctuations ξ. The consistency of $I(q)$ in these two gels in the high-q region is reasonable, as thermodynamic fluctuations mainly

Table 3.1: Estimated size of the spatial defects ($R_{g,z}$) and the correlation blob (ξ) in each gel, as well as the corresponding scattering intensities $I_G(0)$ and $I_{OZ}(0)$, respectively. The errors represent the fitting error.

	Bond percolation	Non-ideal bond percolation	site percolation
$I_{OZ}(0)$ [cm^{-1}]	0.27 ($\pm$0.01)	0.27 ($\pm$0.01)	0.37 ($\pm$0.01)
ξ [nm]	0.9 ($\pm$0.1)	0.9 ($\pm$0.1)	2.4 ($\pm$0.1)
$I_G(0)$ [cm^{-1}]	N.A.	1.67 ($\pm$0.1)	0.52 ($\pm$0.1)
$R_{g,z}$ [nm]	N.A.	53.6 ($\pm$9.1)	7.1 ($\pm$0.8)

depend on the polymer concentration [71], which was identical for these two gels. However, an additional shoulder was observed in the low-q region ($q \approx 0.01$ nm^{-1}) in the $I(q)$ profile of the non-ideal bond percolation gel. This additional shoulder was attributed to spatial defects, the presence of which was confirmed in the static laser speckle images (Fig. 3.6(B), (E)). To estimate the size of the spatial defects, I subtracted the contribution of the thermodynamic fluctuations, i.e., the OZ model curve, from the $I(q)$ profile and fitted the low-q region of the $I(q)$ plot using the Guinier equation:

$$I(q) = I_{\mathrm{G}}(0) \exp\left(-\frac{R_{g,z}^2 q^2}{3}\right) \tag{3.5}$$

where $I_{\mathrm{G}}(0)$ is the intensity at $q = 0$ from the Guinier equation and $R_{g,z}$ is the z-average gyration radius of the spatial defects (Fig. 3.10(B)) [46, 72]. The obtained fit parameters are summarized in Table 3.1. The estimated defect size in the non-ideal bond percolation gel was approximately 54 nm, which was much higher than the size of a star polymer unit in the pre-gel solution ($R_g \approx 3.5$ nm).

The volume fraction of the defects can be estimated by combining the value of $I_{\mathrm{G}}(0)$ and the crosslinking ratio, which was estimated from the mechanical tests. If I assume that the defects are uniform spheres with a constant local polymer concentration that is either higher or lower than that of the surrounding gel network, $I_{\mathrm{G}}(0)$ can be expressed as a function of the volume fraction of the spatial defects (Φ_{def}):

$$I_{\mathrm{G}}(0) = \Delta\rho^2 \Phi_{\mathrm{def}} \frac{4\pi}{3} R_{g,z}^3 \tag{3.6}$$

Here, $\Delta\rho$ is the difference between the scattering length density of the defects and the gel network, which is a function of Φ_{def} and the local polymer volume fraction (ϕ_{local}) (for the derivation, see the Appendix), and can be expressed as:

$$\Delta\rho = (\rho_{\mathrm{p}} - \rho_{\mathrm{s}})\frac{\phi_{\mathrm{local}} - \phi}{1 - \Phi_{\mathrm{def}}} \tag{3.7}$$

Here, ρ_{p} and ρ_{s} represent the scattering length density of the polymers and solvent molecules, respectively. The number fraction of star polymer units participating in the spatial defects (n_{def}) can also be written as a function of Φ_{def} and ϕ_{local}:

$$n_{\mathrm{def}} = \Phi_{\mathrm{def}} \frac{\phi_{\mathrm{local}}}{\phi} \tag{3.8}$$

The results of the mechanical tests suggest that the crosslinking ratio of the non-ideal bond percolation gel is 5% lower than that of the bond percolation gel, thus indicating that 5% of the initial star polymer units were not fully integrated into the network in the non-ideal bond percolation gel compared to the bond percolation gel. Assuming that these polymer units all formed aggregates, n_{def} can be roughly

estimated to be 5%. By combining eq (3.6), eq (3.7), and eq (3.8) and substituting the values of n_{def} and $I_{\text{G}}(0)$, Φ_{def} and ϕ_{local} were estimated to be 0.046 and 0.105, respectively (for details of the calculation, see the Appendix). The estimated ϕ_{local} was higher than that of the surrounding environment ($\phi = 0.096$), confirming the formation of polymer-rich defects, i.e., polymer aggregates, in the non-ideal bond percolation gel. The concentration of PEG in the aggregates was only ~10% higher than that of the surrounding environment, suggesting that the density of aggregates was relatively low. The existence of such aggregates, which had been postulated in previous studies of PEGs dissolved in water [37], was experimentally confirmed in this study for the first time. In summary, by lowering the affinity between the solvent and polymer chains, I successfully doped the gel with nanosized polymer aggregates (radius:~50 nm). The aggregates occupied ~5 vol% of the gel, and the concentration of the polymer in the aggregates was only 10% higher than in the surrounding environment.

Unlike the clear signature of the spatial defects observed in the non-ideal bond percolation gel, the site percolation gel had only one shoulder in its $I(q)$ profile at $q = 0.1 - 0.2$ nm^{-1} (Fig. 3.7). This is likely due to the size of these spatial defects, which is similar to the size of the thermodynamic fluctuations, ξ, in this gel. The theoretical value of ξ in the site percolation gel (2.4 nm) was estimated from the theoretical scaling relation for a crowded polymer solution [71] ($\xi \sim \phi^{-3/4}$) and the ξ value of the bond percolation gel ($\xi = 0.909$ nm, see Table 3.1) using the value of $\phi = 0.0259$ for site percolation gel and $\phi = 0.0961$ for bond percolation gel. The OZ model curve (eq (3.4)) calculated using $\xi = 2.4$ nm was in perfect agreement with the $I(q)$ of the site percolation gel in the high-q region (Fig. 3.9), confirming the reliability of the theoretical estimation of ξ. In this calculation, the relation of $I_{\text{OZ}}(0) = A'\phi^2\xi^3$, where A' is a proportionality constant, was used. Based on eq (3.4), I normalized the contribution of thermodynamic fluctuations to the scattering profiles by plotting $I(q) \cdot \phi^{-2}\xi^{-3}$ as a function of $q\xi$ (Fig. 3.7(B)) to visualize the excess intensity due to the spatial defects in the site percolation gel. While the normalized profile of the bond percolation gel agreed with the OZ model curve over the entire q range, clear deviations from the OZ model curve were observed in the site percolation gel at low q ($q < 0.1$ Å^{-1}) as well as for the non-ideal bond percolation gel (vide supra). The deviation of the scattering profile from the OZ model curve confirmed the presence of spatial defects in the site percolation gel. I subtracted the OZ model curve from the $I(q)$ of the site percolation gel and then fitted the residual using the Guinier equation (eq (3.5)) to estimate the size and the volume fraction of the spatial defects, i.e., voids, in the site percolation gel (Fig. 3.10(A); fitting parameters are listed in Table 3.1). The radius of the spatial defects was estimated to be 7.1 nm, which was approximately twice the size of the star polymer unit ($R_g \approx 3.5$ nm).

The volume fraction of the spatial defects, Φ_{def}, in the site percolation gel was estimated using eq (3.6) and eq (3.7) to be $\sim 26\%$ of the total gel volume by assuming that the spatial defects are voids with a local polymer fraction ϕ_{local} of zero (for details of the calculation, see the Appendix). The high volume fraction of the voids is reasonable, as the star polymer units covered only approximately half of the space in the initial pre-gel solution ($c = 1.5$ mM $\sim$ c*/2). The prevalence of nanovoids within the gel network is likely responsible for the decreased crosslinking conversion and elastic modulus in the site percolation gel as seen in the mechanical tests. In summary, by releasing the geometric constraints in the pre-gel solution, I successfully introduced nanosized voids with an average size of 7 nm occupying 26 vol% of the gel.

In addition to investigating the parameters of the spatial defects from a static point of view, I also evaluated these defects in terms of temporal correlations using the time-averaged intensity correlation functions $g_{\text{T}}^{(2)}(\tau)$ measured using DLS. Here, $g_{\text{T}}^{(2)}(\tau)$ is defined as:

$$g_{\text{T}}^{(2)}(\tau) - 1 = \frac{\langle I(0)I(\tau)\rangle_{\text{T}}}{\langle I \rangle_{\text{T}}^2} - 1 = \alpha \exp(-2D_{\text{A}}q^2\tau) \tag{3.9}$$

where τ is the lag time of a temporal correlation, α is an instrument-dependent parameter, and D_{A} is the apparent diffusion coefficient [42, 50, 73]. As polymer gels are non-ergodic materials, the dynamics of the polymer chains may vary from position to position. To evaluate both the local and ensemble-averaged dynamics, I measured each gel sample at 100 different, randomly chosen sample positions.

The time-averaged scattering intensity, $\langle I \rangle_{\text{T}}$, at each sample position is shown in Fig. 3.11(A). The solid lines show the ensemble-averaged scattering intensity $\langle I \rangle_{\text{E}}$, which was calculated by averaging the $\langle I \rangle_{\text{T}}$ values at different sample positions, i.e., $\langle I \rangle_{\text{E}} = \langle\langle I \rangle_{\text{T}}\rangle_{\text{E}}$. In the bond percolation gel, $\langle I \rangle_{\text{T}}$ was independent of the sample position, confirming the high spatial homogeneity in this gel. In contrast, in the site percolation and non-ideal bond percolation gels, $\langle I \rangle_{\text{T}}$ varied randomly at different positions, confirming the successful doping of these gels with spatial defects.

Fig. 3.11(B) shows the $g_{\text{T}}^{(2)}(\tau)$ curves at the 100 different sample positions. For the bond percolation gel, all the $g_{\text{T}}^{(2)}(\tau)$ curves overlap well with each other. The curve of the ensemble-averaged correlation function $g_{\text{E}}^{(2)}(\tau)$, which was calculated by averaging the $g_{\text{T}}^{(2)}(\tau)$ curves, is also in good agreement with the individual local $g_{\text{T}}^{(2)}(\tau)$ curves. Here, $g_{\text{E}}^{(2)}(\tau)$ is defined by:

$$g_{\text{E}}^{(2)}(\tau) \equiv \frac{\langle I(0)I(\tau)\rangle_{\text{E}}}{\langle I \rangle_{\text{E}}^2} = \frac{\langle\langle I(0)I(\tau)\rangle_{\text{T}}\rangle_{\text{E}}}{\langle I \rangle_{\text{E}}^2} \tag{3.10}$$

With the definition of $g_{\text{T}}^{(2)}(\tau)$ (eq (3.9)), the ensemble-averaged correlation function
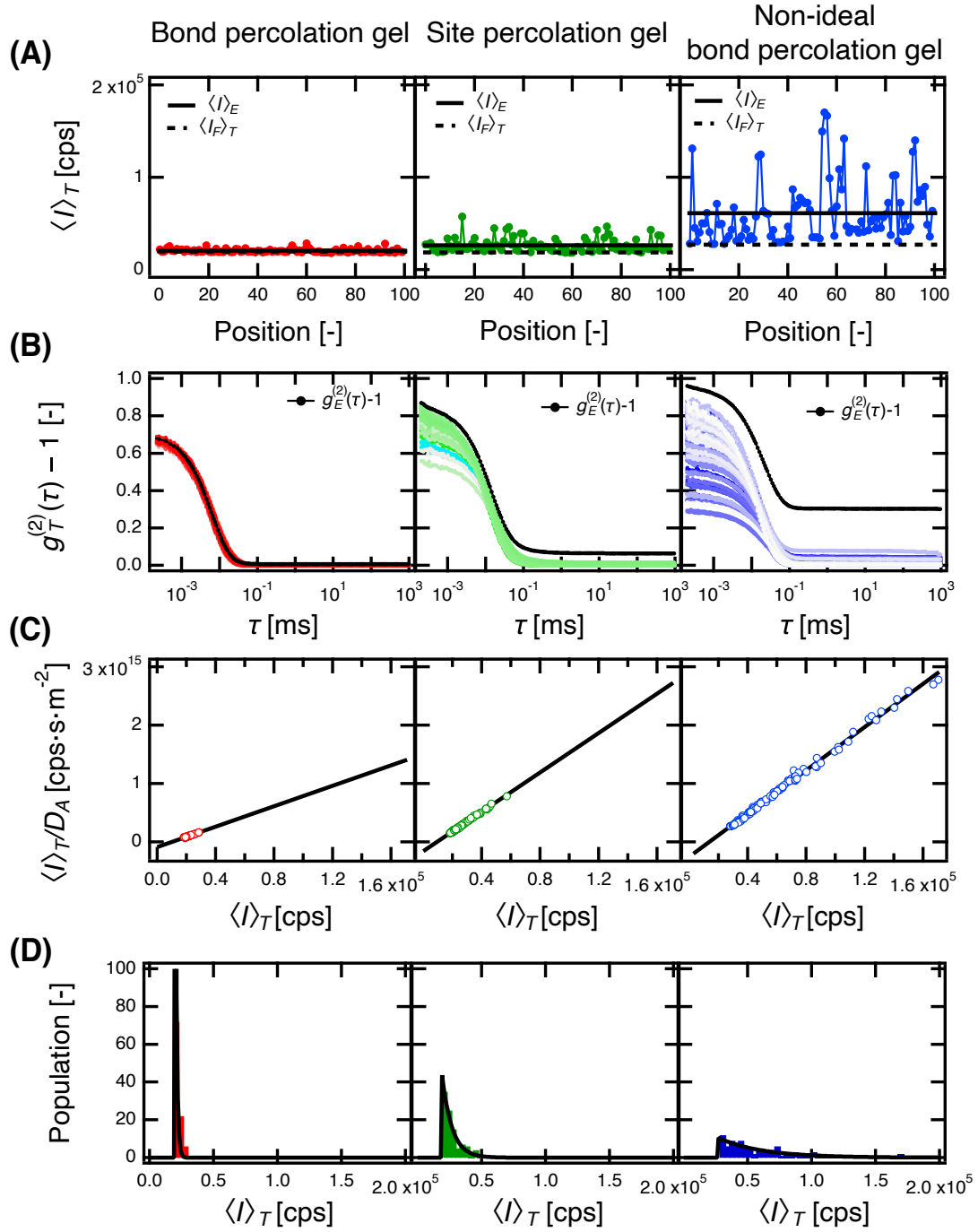
Figure 3.11: Dynamic properties of the fully developed gels synthesized under various percolation conditions. (A) Time-averaged scattered intensity $\langle I \rangle_T$ at different sample positions. Solid lines represent the ensemble-averaged scattered intensity $\langle I \rangle_E$ and the dashed lines represent its dynamic component $\langle I_F \rangle_T$. (B) Intensity correlation functions $(g_T^{(2)}(\tau)-1)$ at 100 different sample positions and the ensemble-averaged correlation function $(g_E^{(2)}(\tau)-1)$. (C) Partial heterodyne plots $(\langle I \rangle_T / D_A$ vs $\langle I \rangle_T)$. Solid lines represent the fitting with eq (3.13). (D) Population histogram of $\langle I \rangle_T$ obtained by sorting the data in Fig. 3.11(A). Solid curves are the plots predicted from the $\langle I_F \rangle_T$ and $\langle I_C \rangle_T$ values listed in Table 3.2 using eq (3.14).

is described as:

$$g_{\text{E}}^{(2)}(\tau) = \frac{\langle \langle I \rangle_{\text{T}}^2 g_{\text{T}}^{(2)}(\tau) \rangle_{\text{E}}}{\langle I \rangle_{\text{E}}^2} \tag{3.11}$$

These results indicate uniform temporal correlations in this spatially bond percolation gel. A constant deviation of the initial value, $g_{\text{T}}^{(2)}(0)$, from unity is due to instrumentation factors, such as background intensity, which are independent of the sample positions [74].

In contrast to the perfect consistency of $g_{\text{T}}^{(2)}(\tau)$ in the bond percolation gel, the $g_{\text{T}}^{(2)}(\tau)$ curves of the site percolation and non-ideal bond percolation gels vary depending on the sample position, and are not consistent with the ensemble-averaged correlation function $g_{\text{E}}^{(2)}(\tau)$. In addition, the $g_{\text{E}}^{(2)}(\tau)$ curves of the site percolation and non-ideal bond percolation gels did not fully relax within the measurement time, suggesting that these gels contain static components and/or very slowly relaxing components. The static components must originate from the spatial defects in the gels, as they were only observed in the gels containing spatial defects. In the site percolation gel, the static component was attributed to the nanovoids, as they cannot relocate once the gel network has fully developed. On the other hand, in the non-ideal bond percolation gel, the nanosized soft aggregates of polymer chains were likely the origin of the static components, as they were much larger than the mesh size and thus were likely entrapped by the gel network.

I hypothesized that the non-ideal bond percolation and site percolation gels contained a fully static component in addition to the fully dynamic component observed in the bond percolation gel. This is known as the partial heterodyne model; the corresponding expression for $g_{\text{T}}^{(2)}(\tau)$ at each sample position is [50]:

$$g_{\text{T}}^{(2)}(\tau) - 1 = \alpha[X^2 \exp(-2D_{\text{F}}q^2\tau) + 2X(1-X)\exp(-D_{\text{F}}q^2\tau)] \tag{3.12}$$

where $X \equiv \langle I_{\text{F}} \rangle_{\text{T}} / \langle I \rangle_{\text{T}}$ is the ratio of the intensity that originates from the dynamic

Table 3.2: Estimated diffusion coefficient of the dynamic component (D_{F}), the screening length of the hydrodynamic interactions between the segments in the polymer chains (ξ_{h}), the ensemble-averaged scattering intensity ($\langle I \rangle_{\text{E}}$) and its dynamic component ($\langle I_{\text{F}} \rangle_{\text{T}}$) as well as its static component ($\langle I_{\text{C}} \rangle_{\text{E}}$) for each gel sample. The errors of D_{F}, ξ_{h} and $\langle I_{\text{F}} \rangle_{\text{T}}$ represent the fitting error. The errors of $\langle I \rangle_{\text{E}}$ and $\langle I_{\text{C}} \rangle_{\text{E}}$ represent the standard error of sample mean.

	Bond percolation	Non-ideal bond percolation	site percolation
D_{F} [$\times 10^{-10}$m^2/s]	2.29 ($\pm$0.03)	1.08 ($\pm$0.01)	1.19 ($\pm$0.01)
ξ_{h} [nm]	2.81 ($\pm$0.04)	2.27 ($\pm$0.02)	5.42 ($\pm$0.04)
$\langle I \rangle_{\text{E}}$ [$\times 10^4$cps]	2.07 ($\pm$0.02)	6.11 ($\pm$0.33)	2.64 ($\pm$0.08)
$\langle I_{\text{F}} \rangle_{\text{T}}$ [$\times 10^4$cps]	1.97 ($\pm$0.06)	2.71 ($\pm$0.10)	1.87 ($\pm$0.04)
$\langle I_{\text{C}} \rangle_{\text{E}}$ [$\times 10^4$cps]	0.10 ($\pm$0.06)	3.40 ($\pm$0.34)	0.77 ($\pm$0.09)

component, $\langle I_F \rangle_T$, to the total intensity, $\langle I \rangle_T$, at each sample position, and D_F is the diffusion coefficient of the dynamic component. By combining eq (3.9) and eq (3.12) and then performing a Taylor expansion, the following relationship is obtained for each sample position [73, 75]:

$$\frac{\langle I \rangle_T}{D_A} = \frac{2}{D_F}\langle I \rangle_T - \frac{\langle I_F \rangle_T}{D_F} \tag{3.13}$$

Based on this equation, I organized the 100 data sets for each gel shown in Fig. 3.11(A) and (B) and replotted $\langle I \rangle_T/D_A$ as a function of $\langle I \rangle_T$ for each sample position (Fig. 3.11(C)). The data points from different sample positions all fell on a master line for each gel, suggesting that the partial heterodyne model is applicable. The slope and intercept in Fig. 3.11(C) furnish D_F and $\langle I_F \rangle_T$, respectively. The obtained parameters are listed in Table 3.2.

The values of D_F ($1-3 \times 10^{-10}$ m^2/s) are consistent with the thermal concentration fluctuations of the polymer chains in a semidilute solution [36, 76–78]. The size of the concentration fluctuations, or the screening length of the hydrodynamic interactions between the segments in the polymer chains, ξ_h, was estimated from D_F using the Stokes-Einstein equation, $\xi_h = kT/6\pi\eta D_F$, where k is the Boltzmann constant, T is the absolute temperature, and η is the viscosity of the solvent [71]. The obtained values of ξ_h are 2-3 times higher than those of ξ (Table 3.1), which is consistent with previous studies of crowded polymer solutions [79–81]. Such differences between ξ_h and ξ have been predicted theoretically and been attributed to the difference between the hydrodynamic interaction and the excluded volume effect, whereby the former decays more slowly than the latter [82]. As all the data points measured at different sample positions converged on a single line (Fig. 3.11(C)), only one slope, i.e., D_F and one intercept, i.e., $\langle I_F \rangle_T$ were obtained for each gel. The positional independence of D_F and $\langle I_F \rangle_T$ indicates that the concentration fluctuations of polymers are an inherent property of gels that is insensitive to the type and the number of spatial defects, i.e., $D_F = \langle D_F \rangle_E$ and $\langle I_F \rangle_T = \langle I_F \rangle_E$.

The estimated position-independent $\langle I_F \rangle_T$ value of each gel is indicated in Fig. 3.11(A). The $\langle I_F \rangle_T$ and $\langle I \rangle_E$ values of the bond percolation gel are identical within the experimental error, suggesting that there is almost no static component $\langle I_C \rangle_E = \langle I \rangle_E - \langle I_F \rangle_E$ in this gel. In contrast, for the site percolation and non-ideal bond percolation gels, $\langle I_F \rangle_T$ is lower than $\langle I \rangle_E$, indicating the presence of a static component. In addition, the $\langle I_F \rangle_T$ of the site percolation and non-ideal bond percolation gels is obviously the minimum value of the randomly varying $\langle I \rangle_T$ in each gel, suggesting that the extent of the static component differs at different positions, i.e., $\langle I_C \rangle_T \neq \langle I_C \rangle_E$. As discussed above, the static component in the gels must be attributed to the spatial defects. Therefore, the position-dependent behavior of the static component suggests a random distribution of the spatial defects in these gels. I sorted the intensities at each position to create a population histogram

(Fig. 3.11(D)). The population histograms are exponential with cut-offs at low $\langle I \rangle_{\mathrm{T}}$ values. Similar distributions have been reported in previous studies and analyzed using a negative exponential distribution with an offset ($P(\langle I \rangle_{\mathrm{T}})$) [38, 83]:

$$P(\langle I \rangle_{\mathrm{T}}) = a \frac{H(\langle I \rangle_{\mathrm{T}} - \langle I_{\mathrm{F}} \rangle_{\mathrm{T}})}{\langle I_{\mathrm{C}} \rangle_{\mathrm{E}}} \exp\left(-\frac{\langle I \rangle_{\mathrm{T}} - \langle I_{\mathrm{F}} \rangle_{\mathrm{T}}}{\langle I_{\mathrm{C}} \rangle_{\mathrm{E}}} \right) \tag{3.14}$$

where a is a scale factor equal to the total area of the histogram, $H(x)$ is the Heaviside function, which gives 0 for $x < 0$ and 1 for $0 \leqq x$, respectively. The theoretical $P(\langle I \rangle_{\mathrm{T}})$ plots calculated using eq (3.14) and the values in Table 3.2 are plotted in Fig. 3.11(D) and are in good agreement with the measured histograms. The exponential frequency distribution of the scattering intensity is a common statistical feature of systems with randomly distributed static scattering components, such as the rough surface of a piece of ground glass [84]. Therefore, it is reasonable to observe exponential distributions of the scattering intensities from gels with spatial defects. The observed offset scattering intensity is equal to $\langle I_{\mathrm{F}} \rangle_{\mathrm{T}}$, indicating that the offset originates from the concentration fluctuations of the polymer chains. The negative exponential distribution and the partial heterodyne mode suggest that the induced nanosized spatial defects are randomly distributed in a dynamically fluctuating gel network with uniform fluctuations that are insensitive to the parameters of the spatial defects.

3.4   Conclusion

Here, I have demonstrated the fabrication of gels that were selectively induced spatial defects by tuning the percolation process, that is, an affinity of solvent and a total polymer concentration. While the formation of spatial defects is greatly reduced using the bond percolation process, nanosized voids and aggregates can be selectively introduced via site percolation and non-ideal bond percolation processes.

To demonstrate the incorporation of the spatial heterogeneity, I examined the structure of the bond percolation gel, the site percolation gel, and the non-ideal percolation gel with multiple methods, dynamic mechanical analysis, 2D laser speckle imaging, static light, and X-ray scattering, and dynamic light scattering. G' of the site percolation gel suggested the existence of elastic defects, and this was more in number than these of the other gels, which was caused by the low packing effects. 2D laser speckle imaging showed the presence of spatial defects in the site percolation gel and the non-ideal bond percolation gel. The brightness of speckles depended on the size of spatial defects. SAXS experiments give us information about the size and the volume fraction of spatial defects. R_g of aggregations in the non-ideal percolation gel was about 54 nm, which was bigger than R_g of voids, which leads difference in the brightness of the speckle. The estimated volume fraction of the site percolation gel was larger than that of the non-ideal bond percolation gel. Es-

timated $I(0)$ and ξ from the bond percolation gel or the non-ideal percolation gel based on the scaling law reproduced the concentration fluctuation of the site percolation gel in SAXS. Regarding heterogeneities quantified as the scattered intensity with DLS, static components of the non-ideal bond percolation gel is larger than the site percolation gel regardless of the volume fraction of defects given with SAXS. This is reasonable because the intensity of light scattering increases as the radius of scattering elements becomes big.

In this study, I succeeded the selective doping of spatial heterogeneity into the gel network based on the bond percolation concept. To the best of my knowledge, the spatial defects in gels have never been precisely controlled and have always created disorder within the gels. In addition to the significant change in the optical and mechanical properties in the gels introduced by the spatial defects, the nanodefects may also effectively regulate the mass transportation in gels, such as entropic trapping in the nanovoids and obstacle retardation by the nanoaggregates. The present strategy does not depend on the specific chemistry of the polymers and crosslinking reactions, which further expands the range of potential applications. Furthermore, results obtained here support the effectiveness of the bond percolation concept to fabricate spatial homogeneous gels. Hence, it is possible to control spatial heterogeneity irrespective of the chemistry of the polymers using this concept.

Since chapters 4 to 6 contain the unpublished data, these chapters were removed.

CHAPTER 7

General conclusion

In my doctoral dissertation, I focused on static and dynamic structural analysis of spatial homogeneous model network gels under deformation. The main analysis method was scattering, where probes were neutron, X-ray, and light.

The basis of these studies is the establishment of the synthesis of spatial homogeneous gel. This synthesis is based on the bond percolation concept. This concept is not limited to the specific polymer species and universal concept: the end-linking of polymer with stronger excluded volume effect at higher polymer concentration above the overlapping concentration (concentration condition) in a high-affinity solvent (solvent condition). This is based on the idea that lower polymer concentration induces the production of nano-voids, and poor-affinity solvent induces polymer aggregation. This means that heterogeneities could be incorporated into gel networks by removing these conditions on purpose. In chapter 3, in accordance with the idea of the bond percolation concept, two types of heterogeneities, i.e., polymer aggregations and nano-voids, were incorporated into the gel network by independently removing the concentration and solvent condition. The existence of heterogeneities was confirmed from the scattering method in both static and dynamic perspectives. Moreover, the quantitative evaluation of heterogeneities was conducted, and the results were reasonable. This study supported the effectiveness of the bond percolation concept was demonstrated robustly.

In the following chapters, I investigated the structure of model network gels under deformation with the scattering techniques. To extract the universal structural properties of gels under deformation, it is essential to remove the influence of heterogeneity, especially spatial heterogeneity, which has a strong scattering contribution. In these studies, the synthesis scheme based on the bond percolation concept was adopted to fabricate spatial homogeneous model network gels.

In chapter 4, the static structural analysis of the model network gel under elongation was conducted with small-angle X-ray scattering. Here, the reaction efficiency was tuned to elucidate the effect of bond defects for the structure under elonga-

tion. Anisotropic 2D scattering profiles appeared with elongation when the reaction efficiency was high. This anisotropic scattering pattern was similar to the abnormal butterfly pattern, which is typical for the conventional static heterogeneous gels. The abnormal butterfly pattern is usually explained due to the spatial heterogeneity in theory. However, in the case of our study, the reproductivity of the scattering profiles for multiple sample pieces was confirmed. This result suggests that our anisotropic pattern might not originate from the spatial heterogeneity induced elongation but the stretching of polymer strands with elongation. It is because heterogeneity should depend on positions, that is, sample pieces. This anisotropic pattern disappeared with a reduction of the reaction efficiency. This result also supports the above argument.

In chapter 5, the static structural analysis of the model network gel under compression was conducted with small-angle neutron scattering (SANS). The advantage of neutron scattering, i.e., isotope labeling, was used to observe polymer segments around a cross-linking point and vice versa. While the non-labeled gels did not show any distinct change with compression for the scattering profiles, the labeled gels for segments around cross-linking point or strands between cross-linking point indicated the apparent maximum intensity at the specific magnitude of scattering vector q and position of maximum point moved into smaller q with compression. This result demonstrated the powerfulness of isotope labeling for the structural analysis of gels under deformation. The model-fitting analysis with the random phase approximation provided the characteristic quantity of the network deformation. This variation trend with compression of this quantity is well consistent with the previous study, which indicates that the phantom-like behavior of chains of gels under deformation is an intrinsic property irrespective of spatial heterogeneity.

In chapter 6, the dynamic structural analysis of the model network gel under compression was conducted with quasi-elastic neutron scattering (QENS). As same with chapter 5, the feature of neutron scattering was taken advantage, and the isotope labeling was used. It should be noted that hydrogen-labeled parts are important in QENS as different from SANS to observe the self-diffusion. In this study, the dynamics for different orientation was collected because the network structure of compressed gels is anisotropic. There was no distinct difference of dynamics depending on the labeled parts. However, the orientation dependence of the dynamics change with compression was observed, i.e., while the in-plane dynamics were close to the segmental dynamics of non-compressed gels, the out-of-plane dynamics changed faster. Although this is considered due to the solvation structural change with compression, the detailed mechanism is not clear currently. To explore the molecular origin of this change, further investigation is necessary.

In this doctoral dissertation, I first established the synthesis strategy of the model network gels based on the simple and the non-constrained by polymer species con-

cept. Spatial heterogeneity had been a long-standing problem in gel science, which hinders the understanding of the structural property of gels. I proposed the solution for this problem in this dissertation and demonstrated the utility of such gels for structural analysis with scattering methods. I conducted the structural analysis for spatial homogeneous model network gels in various aspects, and the results contributed to the understanding of the universal properties of gels under deformation through structural analysis with scattering methods.

Appendix

1 Estimation of the volume fraction and local concentration of aggregates and nano-voids in gel networks

The scattering intensity at $q \to 0$, $I_G(0)$, for an arbitrary object at low concentration is given by:

$$I_G(0) = \Delta\rho^2 \Phi v \tag{7.1}$$

where $\Delta\rho$ is the difference between the scattering length density (SLD) of the object and the medium, Φ is the volume fraction of the object, and v is the volume of the object [41]. Accordingly, we modelled the spatial defects as spherical objects with a radius R:

$$v = \frac{4}{3}\pi R^3 \tag{7.2}$$

We assumed that the defects had a uniform SLD with higher or lower value than that of the surrounding gel network. The difference between the SLD of the defects (ρ_{def}) and the gel network (ρ_{gel}) is given by:

$$\Delta\rho = \rho_{\mathrm{def}} - \rho_{\mathrm{gel}} \tag{7.3}$$

The SLDs of the defects and the gel network are:

$$\rho_{\mathrm{def}} = \phi_{\mathrm{local}}\rho_{\mathrm{p}} + (1 - \phi_{\mathrm{local}})\rho_{\mathrm{s}} \tag{7.4}$$

$$\rho_{\mathrm{gel}} = \phi_{\mathrm{global}}\rho_{\mathrm{p}} + (1 - \phi_{\mathrm{global}})\rho_{\mathrm{s}} \tag{7.5}$$

Here, ρ_{p} and ρ_{s} are the SLD of the polymer and solvent, respectively, while ϕ_{local} and ϕ_{global} are the polymer volume fraction in the defects and in the gel network, respectively. As the total polymer volume fraction (ϕ) in the gel is constant, the following conservation law applies:

$$\phi = \phi_{\mathrm{local}}\Phi_{\mathrm{def}} + \phi_{\mathrm{global}}(1 - \Phi_{\mathrm{def}}) \tag{7.6}$$

Where Φ_{def} is the volume fraction of the defects in the total gel volume. By com-

bining the above equations, we obtain:

$$\Delta\rho = (\rho_{\mathrm{p}} - \rho_{\mathrm{s}})(\phi_{\mathrm{local}} - \phi_{\mathrm{global}}) = (\rho_{\mathrm{p}} - \rho_{\mathrm{s}})\left(\frac{\phi_{\mathrm{local}} - \phi}{1 - \Phi_{\mathrm{def}}}\right) \tag{7.7}$$

By substituting eq. (7.7) and eq. (7.6) into eq. (7.1), $I_G(0)$ can be rewritten as:

$$I_G(0) = (\rho_{\mathrm{p}} - \rho_{\mathrm{s}})^2 \left(\frac{\phi_{\mathrm{local}} - \phi}{1 - \Phi_{\mathrm{def}}}\right)^2 \Phi_{\mathrm{def}} \frac{4}{3}\pi R^3 \tag{7.8}$$

Here, ρ_{p}, ρ_{p}, and ϕ are the known values in chapter 3, and $I_G(0)$ and R were estimated from the scattering profiles and listed in Table 3.1 in chapter 3. Therefore, in the above equation, Φ_{def} and ϕ_{local} are the only undetermined parameters.

1.1 For the site percolation gel

If we assume that the polymer volume fraction in the nano-voids is 0, i.e., $\phi_{\mathrm{local}} = 0$, eq. (7.8) becomes:

$$I_G(0) = (\rho_{\mathrm{p}} - \rho_{\mathrm{s}})^2 \left(\frac{\phi}{1 - \Phi_{\mathrm{def}}}\right)^2 \Phi_{\mathrm{def}} \frac{4}{3}\pi R^3 \tag{7.9}$$

By substituting the known parameters and the $I_G(0)$ and R values obtained from the scattering profile of the site percolation gel, we obtain:

$$\Phi_{\mathrm{def}} = 0.256 \tag{7.10}$$

1.2 For the non-ideal bond percolation gel

The ϕ_{local} of the aggregates is an unknown parameter, and additional information is required to solve eq. (7.8). Here, we build another equation for ϕ_{local} and Φ_{def}. The total volume of PEG in the gel is:

$$V_{\mathrm{p}} = V\phi \tag{7.11}$$

where V is the total gel volume. The total PEG volume in the spatial defects is given by:

$$V_{\mathrm{PEG_{def}}} = V\Phi_{\mathrm{def}}\phi_{\mathrm{local}} \tag{7.12}$$

Therefore, the volume fraction of PEG in the defects relative to the total PEG volume, which is equivalent to the number fraction of tetra-PEG units in the defects (n_{def}), can be written as:

$$n_{\mathrm{def}} = \frac{V_{\mathrm{PEG_{def}}}}{V_{\mathrm{p}}} = \frac{\Phi_{\mathrm{def}}\phi_{\mathrm{local}}}{\phi} \tag{7.13}$$

As is discussed in chapter 3, n_{def} can be estimated based on the mechanical measurements. Then, by simultaneously solving equations eq. (7.13) and eq. (7.8) using the n_{def} and $I_G(0)$ values obtained from the scattering measurements, we obtain:

$$\phi_{\text{local}} = 0.105 \tag{7.14}$$

$$\Phi_{\text{def}} = 0.046 \tag{7.15}$$

2 Random pahse approximation for the three conponent system

I consider the system composed of two polymers, hydrogenated and deuterated one, in the solvent. According to Benoit et al. [85,86], random phase approximation gives the scattering intensity as

$$
\begin{aligned}
I(q) = A_0 [&\Delta\rho_H^2 S_{HH}^0 + \Delta\rho_D^2 S_{DD}^0 + 2\Delta\rho_H \Delta\rho_D S_{HD}^0 \\
&+ (S_{HH}^0 S_{DD}^0 - S_{HD}^{0\,2})(\Delta\rho_H^2 v_D + \Delta\rho_D^2 v_{HH} - 2\Delta\rho_H \Delta\rho_D v_{HD})] \\
[1 &+ v_{HH} S_{HH}^0 + v_D S_{DD}^0 + 2v_{HD} S_{HD}^0 + (v_{HH}v_{DD} - v_{HD}^2)(S_{HH}^0 S_{DD}^0 - S_{HD}^{0\,2})]^{-1}
\end{aligned} \tag{7.16}
$$

where A_0, $\Delta\rho_{\text{x}}$, S_{xx}^0, and v_{xx} (x = H or D) are the prefactor, the difference between the scattering length density of a polymer and a solvent, the bare structure factor, and the excluded volume parameter, respectively. $\Delta\rho_{\text{x}}$ is defined as

$$\Delta\rho_{\text{x}} = \rho_{\text{x}} - \rho_{\text{solvent}} \tag{7.17}$$

Here x is the scattering length density of hydrogenated or deuterated polymer.

2.1 Solution

In the eq. (7.16), functions of q, S_{xx}^0 and v_{xx}, are involved. The definition of these functions is described in this section.

First, we consider the mixture solution of the deuterated linear PEG and the hydrogenated 4-arm PEG. The bare structure factors S_{xx}^0 are defined using the molecular form factor $P(q)$ as

$$S_{HH}^0 = N_H \phi_H V_H P_4(q) \tag{7.18}$$

$$S_{DD}^0 = N_D \phi_D V_D P_2(q) \tag{7.19}$$

$$S_{HD}^0 = 0 \tag{7.20}$$

where N_{x}, ϕ_{x}, V_{x} are the polymerization degree of the molecule, the polymer volume

fraction, and the molar volume of the monomer, respectively. $P_4(q)$ and $P_2(q)$ is the molecular form factor of gaussian 4-arm star polymer chain and linear chain, respectively. We put g as functional number of a star polymer, then $P_g(q)$ can be written as [87]

$$P_g(q) = (2-g)\frac{2\left[\exp(-u/g)+u/g-1\right]}{u^2} + g(g-1)\frac{\left[\exp(-2/g)+2u/g-1\right]}{u^2} \quad (7.21)$$

Here, $u = q^2 b^2 N/6 = q^2 R_g^2$ where b is the size of the segment and R_g is the radius of gyration. The excluded volume parameter v_{xx} is defined as

$$v_{HH} = \frac{1}{V_s}\left(\frac{1}{1-\phi} - 2\chi_{HS}\right) \quad (7.22)$$

$$v_{DD} = \frac{1}{V_s}\left(\frac{1}{1-\phi} - 2\chi_{DS}\right) \quad (7.23)$$

$$v_{HD} = \frac{1}{V_s}\left(\frac{1}{1-\phi} - \chi_{HS} - \chi_{DS} + \chi_{HD}\right) \quad (7.24)$$

where V_s, ϕ, χ_{xx} are the molar volume of the solvent, the total volume fraction of polymers, and the Flory-Huggins interaction parameter between each component, respectively. In the case of the mixture solution of hydrogenated both 4-arm and linear PEG, each parameter of deuterated PEG is replaced with hydrogenated one except for $P_2(q)$. In this study, we assumed that χ_{HD} was 0.

In the case of the mixture solution of the deuterated linear PEG and the hydrogenated 4-arm PEG, the following numerical values were used.

$$\phi_H = 0.0212[-]$$
$$\phi_D = 0.0551[-]$$
$$N_H = 455[-]$$
$$N_D = 500[-]$$
$$V_H = 6.04 \times 10^{-23}[\text{cm}^3]$$
$$V_D = 7.09 \times 10^{-23}\ [\text{cm}^3]$$
$$V_s = 1.29 \times 10^{-22}\ [\text{cm}^3]$$

As for the mixture solution of hydrogenated both 4-arm PEG and linear PEG,

$$\phi = 0.0763\ [\text{-}]$$

Other parameters were the same with the mixture solution of the deuterated linear PEG and the hydrogenated 4-arm PEG. The fitting parameters were a prefactor A_0, the expansion ratio of the gyration radius α, the Flory-Huggins parameter between h-PEG and d-PEG and solvent, χ_{HS} and χ_{DS}, the segment length of PEG b.

2.2 Gel

Next, we consider the case of gel. Here, as with the previous study [88], we assumed that the structure of gel was the same with that of 4-arm star block copolymer with deuterium labeling on the outer end of each arm, which the segment length of the labeling is half of the linear polymer. If the gel is composed of the deuterated linear PEG and the hydrogenated 4-arm PEG, S^0_{xx} are

$$S^0_{HH} = N_T \phi V_H P_{HH}(q) \tag{7.25}$$

$$S^0_{DD} = N_T \phi V_D P_{DD}(q) \tag{7.26}$$

$$S^0_{HD} = N_T \phi \sqrt{V_H V_D} P_{HD}(q) \tag{7.27}$$

where subscript T denotes the entire star block copolymer. The form factors are defined as [89]

$$P_{HH}(q) = g(2-g)h\left(\frac{1-f_D}{g}\right) + \frac{g(g-1)}{2}h\left(\frac{2(1-f_D)}{g}\right) \tag{7.28}$$

$$P_{DD}(q) = gh\left(\frac{f_D}{g}\right) + \frac{g(g-1)}{2}\left\{h\left(\frac{2}{g}\right) + h\left(\frac{2(1-f_D)}{g}\right) - 2h\left(\frac{2-f_D}{g}\right)\right\} \tag{7.29}$$

$$
\begin{aligned}
P_{HD}(q) = & \frac{g(g-1)}{2}\left\{h\left(\frac{1-f_D}{g}\right) - h\left(\frac{1}{g}\right)\right\} - \frac{g}{2}h\left(\frac{f_D}{g}\right) \\
& + \frac{g(g-1)}{2}\left\{h\left(\frac{2-f_D}{g} - \frac{2(1-f_D)}{g}\right)\right\}
\end{aligned}
\tag{7.30}
$$

Here $h(x)$ is the Leibler function described as

$$h(x) = \frac{2}{u^2}xu + \exp(-xu) - 1 \tag{7.31}$$

and f_D is the fraction of labeling deuterated monomers on the outer end of each arm. It should be noted that $u = q^2 b^2 N_T/6$ in this case.

For the gel composed of only hydrogenated polymer, it is also assumed that the structure of the gel is the same as that of the solution of the 4-arm polymer. Although the form factor of 4-arm polymer is the simple function for gaussian star polymer, eq. (7.21), the length of each arm is longer than the hydrogenated 4-arm polymer (prepolymer) as much as the half of the linear hydrogenated polymer. Thus, it needs to consider only the HH term,

$$S^0_{HH} = N_T \phi V_H P_4(q) \tag{7.32}$$

$$v_{HH} = \frac{1}{V_s}\left(\frac{1}{1-\phi} - 2\chi_{HS}\right) \tag{7.33}$$

In the case of the deuterated labeled gels, the following numerical values were used.

$$f_{\mathrm{D}} = 12/17$$
$$g = 4$$

Other parameters and fitting parameters were the same with the solution.

3 The microscopic chain deformation with macroscopic deformation

In the SANS experiment, we can extract the microscopic deformation with isotope labeling and contrast matching for the radius of gyration R_g. Here, some models which describe the relationship between macroscopic (bulk) deformation and microscopic chain deformation. Here R_{g0} and $R_{g,\mathrm{x}}$ (x = para or perp, i.e., a parallel or perpendicular direction) are the radius of gyration of labeled chain at the undeformed state and that in a parallel and perpendicular direction at the deformed state, respectively.

3.1 Affine network model

In the affine network model, the macroscopic deformation and the microscopic deformation are assumed to be identical. Therefore,

$$R_{g,\mathrm{para}} = \lambda R_{g0} \tag{7.34}$$

$$R_{g,\mathrm{perp}} = \lambda^{-1/2} R_{g0} \tag{7.35}$$

where λ is the macroscopic deformation ratio.

3.2 Phantom network model

In the affine network model, the thermal fluctuation of cross-linkers was suppressed due to the interaction between each polymer segment. On the other hand, in the phantom network model [90], the thermal fluctuation of cross-linkers is considered, and the average position of each cross-linker deforms affinely.

$$R_{g,\mathrm{para}} = \left\{\frac{g + 2 + (g-2)\lambda^2}{2g}\right\}^{1/2} R_{g0} \tag{7.36}$$

$$R_{g,\mathrm{perp}} = \left\{\frac{g + 2 + (g-2)\lambda^{-1}}{2g}\right\}^{1/2} R_{g0} \tag{7.37}$$

where g is the functionality of the cross-linkers.

References

[1] Yoshihito Osada and Jian - Ping Gong. "Soft and Wet Materials: Polymer Gels", . *Adv. Mater.*, 10(11):827–837, 1998.

[2] Thomas Graham. "X. Liquid diffusion applied to analysis", . *Philos. Transactions Royal Soc. Lond.*, 151(151):183–224, 1861.

[3] Dorothy Jordan Lloyd. *Colloid Chemistry; Alexander, J., Ed.* The Chemical Catalog Co., 1926.

[4] P. J. Flory. "Introductory lecture", . *Faraday Discuss. Chem. Soc.*, 57(0):7–18, 1974.

[5] K. Dusek and D. Patterson. "Transition in swollen polymer networks induced by intramolecular condensation", . *J. Polym. Sci. Part A - 2: Polym. Phys.*, 6(7):1209–1216, 1968.

[6] Toyoichi Tanaka. "Collapse of Gels and the Critical Endpoint", . *Phys. Rev. Lett.*, 40(12):820–823, 1978.

[7] Toyoichi Tanaka, David Fillmore, Shao-Tang Sun, Izumi Nishio, Gerald Swislow, and Arati Shah. "Phase Transitions in Ionic Gels", . *Phys. Rev. Lett.*, 45(20):1636–1639, 1980.

[8] Yoshitsugu Hirokawa and Toyoichi Tanaka. "Volume phase transition in a nonionic gel", . *The J. Chem. Phys.*, 81(12):6379–6380, 1984.

[9] H.G. Schild. "Poly(N-isopropylacrylamide): experiment, theory and application", . *Prog. Polym. Sci.*, 17(2):163–249, 1992.

[10] Dirk Schmaljohann. "Thermo- and pH-responsive polymers in drug delivery", . *Adv. Drug Deliv. Rev.*, 58(15):1655–1670, 2006.

[11] Mitsuhiro Shibayama and Toyoichi Tanaka. "Responsive Gels: Volume Transitions I", . *Adv. Polym. Sci.*, pages 1–62, 1993.

[12] "Responsive Gels: Volume Transitions I", . *Adv. Polym. Sci.*, 1993.

[13] "Responsive Gels: Volume Transitions II", . *Adv. Polym. Sci.*, 1993.

[14] F Di Lorenzo and S Seiffert. "Nanostructural heterogeneity in polymer networks and gels", . *Polym. Chem.*, 6(31):5515 – 5528, 2015.

[15] Paul J Flory. "Network Structure and the Elastic Properties of Vulcanized Rubber.", . *Chem. Rev.*, 35(1):51 – 75, 1944.

[16] Paul J. Flory, Norman Rabjohn, and Marcia C. Shaffer. "Dependence of elastic properties of vulcanized rubber on the degree of cross linking", . *J. Polym. Sci.*,

4(3):225–245, 1949.

[17] J. Scanlan. "The effect of network flaws on the elastic properties of vulcanizates", . *J. Polym. Sci.*, 43(142):501–508, 1960.

[18] Thomas Russ, Rüdiger Brenn, and Mark Geoghegan. "Equilibrium Swelling of Polystyrene Networks by Linear Polystyrene", . *Macromolecules.*, 36(1):127–141, 2003.

[19] J. L. Valentîn, J. Carretero-González, I. Mora-Barrantes, W. Chassè, and K. Saalwächter. "Uncertainties in the Determination of Cross-Link Density by Equilibrium Swelling Experiments in Natural Rubber", . *Macromolecules.*, 41(13):4717–4729, 2008.

[20] J E Mark and J L Sullivan. "Model networks of end - linked polydimethylsiloxane chains. I. Comparisons between experimental and theoretical values of the elastic modulus and the equilibrium degree of swelling", . *The J. Chem. Phys.*, 66(3):1006 – 1011, 1977-02.

[21] Yasuyuki Tezuka and Eric J. Goethals. "Synthesis of star and model network polymers from poly(tetrahydrofuran)s with azetidinium end groups and multifunctional carboxylates", . *Die Makromolekulare Chemie*, 188(4):791–797, 1987.

[22] Gerard Hild. "Interpretation of equilibrium swelling data on model networks using affine and 'phantom' network models", . *Polym.*, 38:3279 – 3293, 1997.

[23] Efrosyni Themistou and Costas S. Patrickios. "Synthesis and Characterization of Star Polymers and Cross-Linked Star Polymer Model Networks Containing a Novel, Silicon-Based, Hydrolyzable Cross-Linker", . *Macromolecules.*, 37(18):6734–6743, 2004.

[24] GERARD HILD. "MODEL NETWORKS BASED ON 'ENDLINKING' PROCESSES: SYNTHESIS, STRUCTURE AND PROPERTIES", . *Prog. Polym. Sci.*, 23:1019 – 1149, 08 1998.

[25] Michael Malkoch, Robert Vestberg, Nalini Gupta, Laetitia Mespouille, Philipe Dubois, Andrew F Mason, James L Hedrick, Qi Liao, Curtis W Frank, Kevin Kingsbury, and Craig J Hawker. "Synthesis of well-defined hydrogel networks using Click chemistry", . *Chem. Commun.*, 101(26):2774 – 3, 2006.

[26] Takamasa Sakai, Takuro Matsunaga, Yuji Yamamoto, Chika Ito, Ryo Yoshida, Shigeki Suzuki, Nobuo Sasaki, Mitsuhiro Shibayama, and Ung-il Chung. "Design and Fabrication of a High-Strength Hydrogel with Ideally Homogeneous Network Structure from Tetrahedron-like Macromonomers", . *Macromolecules.*, 41(14):5379 – 5384, 2008-07.

[27] Yuki Akagi, Takuro Matsunaga, Mitsuhiro Shibayama, Ung-il Chung, and Takamasa Sakai. "Evaluation of Topological Defects in Tetra-PEG Gels", . *Macromolecules.*, 43(1):488 – 493, 01 2010.

[28] Yuki Akagi, Takuya Katashima, Yukiteru Katsumoto, Kenta Fujii, Takuro Matsunaga, Ung-il Chung, Mitsuhiro Shibayama, and Takamasa Sakai. "Examina-

tion of the Theories of Rubber Elasticity Using an Ideal Polymer Network", . *Macromolecules.*, 44(14):5817 – 5821, 07 2011.

[29] Yuki Akagi, Jian Ping Gong, Ung-il Chung, and Takamasa Sakai. "Transition between Phantom and Affine Network Model Observed in Polymer Gels with Controlled Network Structure", . *Macromolecules.*, 46(3):1035 – 1040, 01 2013.

[30] Takuya Katashima, Kenji Urayama, Ung-il Chung, and Takamasa Sakai. "Strain energy density function of a near-ideal polymer network estimated by biaxial deformation of Tetra-PEG gel", . *Soft Matter*, 8(31):8217 – 6, 2012.

[31] Xiang Li, Kateryna Khairulina, Ung-il Chung, and Takamasa Sakai. "Migration Behavior of Rodlike dsDNA under Electric Field in Homogeneous Polymer Networks", . *Macromolecules.*, 46(21):8657 – 8663, 10 2013.

[32] Takeshi Fujiyabu, Yuki Yoshikawa, Junhyuk Kim, Naoyuki Sakumichi, Ung-il Chung, and Takamasa Sakai. "Shear Modulus Dependence of the Diffusion Coefficient of a Polymer Network", . *Macromolecules.*, 52(24):9613 – 9619, 12 2019.

[33] Takeshi Fujiyabu, Xiang Li, Ung-il Chung, and Takamasa Sakai. "Diffusion Behavior of Water Molecules in Hydrogels with Controlled Network Structure", . *Macromolecules.*, 52(5):1923 – 1929, 2019-03.

[34] Takashi Yasuda, Naoyuki Sakumichi, Ung-il Chung, and Takamasa Sakai. "Universal Equation of State Describes Osmotic Pressure throughout Gelation Process", . *Phys. Rev. Lett.*, 125(26):267801, 12 2020.

[35] Takuro Matsunaga, Takamasa Sakai, Yuki Akagi, Ung-il Chung, and Mitsuhiro Shibayama. "SANS and SLS Studies on Tetra-Arm PEG Gels in As-Prepared and Swollen States", . *Macromolecules.*, 42(16):6245 – 6252, 08 2009.

[36] Pu Zhou and Wyn Brown. "Static and dynamic properties of poly(ethylene oxide) in methanol", . *Macromolecules.*, 23:1131 – 1139, 1990.

[37] Boualem Hammouda, Derek L Ho, and Steve Kline. "Insight into Clustering in Poly(ethylene oxide) Solutions", . *Macromolecules.*, 37(18):6932 – 6937, 2004-09.

[38] Mitsuhiro Shibayama. "Universality and Specificity of Polymer Gels Viewed by Scattering Methods", . *Bull. Chem. Soc. Jpn.*, 79(12):1799 – 1819, 2006-12.

[39] X. Li, S. Nakagawa, Y. Tsuji, N. Watanabe, and M. Shibayama. "Polymer gel with a flexible and highly ordered three-dimensional network synthesized via bond percolation", . *Sci. Adv.*, 5(12):eaax8647, 11 2019.

[40] Michael Rubinstein and Ralph H Colby. *Polymer Physics.* Oxford University Press. Oxford University Press, 2003.

[41] Ryong-Joon Roe. *Methods of X-ray and Neutron Scattering in Polymer Science.* Oxford University Press. Oxford University Press, 2000.

[42] Bruce J Berne and Robert Pecora. *Dynamic Light Scattering.* Wiley-Interscience. Wiley-Interscience, 1976.

[43] C S Johnson and D A Gabriel. *LASER LIGHT SCATTERING*. Dover. Dover, 1981.

[44] L. R. G. Treloar. *The physics of rubber elasticity*. Clarendon Press, 1975.

[45] Douglas R Miller and Christopher W Macosko. "A New Derivation of Post Gel Properties of Network Polymers", . *Macromolecules.*, 9(2):206 – 211, 1976-03.

[46] Mitsuhiro Shibayama. "Spatial inhomogeneity and dynamic fluctuations of polymer gels", . *Macromol. Chem. Phys.*, 199:1 – 30, 1998.

[47] Simon Mallam, Ferenc Horkay, Anne Marie Hecht, and Erik Geissler. "Scattering and swelling properties of inhomogeneous polyacrylamide gels", . *Macromolecules.*, 22(8):3356 – 3361, 1989-08.

[48] Shin-ichi Takata, Tomohisa Norisuye, and Mitsuhiro Shibayama. "Small-Angle Neutron-Scattering Study on Preparation Temperature Dependence of Thermosensitive Gels", . *Macromolecules.*, 35:4779 – 4784, 2002.

[49] Fumiyoshi Ikkai and Mitsuhiro Shibayama. "Static Inhomogeneities in Thermoreversible Physical Gels", . *Phys. Rev. Lett.*, 82(24):4946 – 4949, 06 1999.

[50] Jacques G H Joosten, Jennifer L McCarthy, and Peter N Pusey. "Dynamic and static light scattering by aqueous polyacrylamide gels", . *Macromolecules.*, 24(25):6690 – 6699, 1991-12.

[51] To Ngai, Chi Wu, and Yun Chen. "Origins of the Speckles and Slow Dynamics of Polymer Gels", . *The J. Phys. Chem. B*, 108(18):5532 – 5540, 2004-05.

[52] Takeshi Karino, Yasushi Okumura, Kohzo Ito, and Mitsuhiro Shibayama. "SANS Studies on Spatial Inhomogeneities of Slide-Ring Gels", . *Macromolecules.*, 37(16):6177 – 6182, 2004-08.

[53] Catherine Rouf-George, Jean-Pierre Munch, François Schosseler, Alain Pouchelon, Gérard Beinert, François Boué, and Jacques Bastide. "Thermal and Quenched Fluctuations of Polymer Concentration in Poly(dimethylsiloxane) Gels", . *Macromolecules.*, 30:8344 – 8359, 1997.

[54] Silvia Corezzi, Daniele Fioretto, and Francesco Sciortino. "Chemical and physical aggregation of small-functionality particles", . *Soft Matter*, 8(44):11207 – 10, 2012.

[55] Antonio Coniglio, H. Eugene Stanley, and W. Klein. "Site-Bond Correlated-Percolation Problem: A Statistical Mechanical Model of Polymer Gelation", . *Phys. Rev. Lett.*, 42(8):518–522, 02 1979.

[56] B Hammouda, D Ho, and S Kline. "SANS from Poly(ethylene oxide)/Water Systems", . *Macromolecules.*, 35(22):8578 – 8585, 2002-10.

[57] Frank Lange, Konrad Schwenke, Manami Kurakazu, Yuki Akagi, Ung-il Chung, Michael Lang, Jens-Uwe Sommer, Takamasa Sakai, and Kay Saalwächter. "Connectivity and Structural Defects in Model Hydrogels: A Combined Proton NMR and Monte Carlo Simulation Study", . *Macromolecules.*, 44(24):9666 – 9674, 12 2011.

[58] Tsutomu Furuya and Tsuyoshi Koga. "Molecular simulation of networks formed by end-linking of tetra-arm star polymers: Effects of network structures on mechanical properties", . *Polym.*, 189:122195, 02 2020.

[59] C Özdemir and A Güner. "Solubility profiles of poly(ethylene glycol)/solvent systems, I: Qualitative comparison of solubility parameter approaches", . *Eur. Polym. J.*, 43(7):3068 – 3093, 2007-07.

[60] H Henning Winter and Francois Chambon. "Analysis of Linear Viscoelasticity of a Crosslinking Polymer at the Gel Point", . *J. Rheol.*, 30(2):367 – 382, 1986-04.

[61] William W Graessley. "Statistical Mechanics of Random Coil Networks", . *Macromolecules.*, 8(2):186 – 190, 1975.

[62] Yui Tsuji, Xiang Li, and Mitsuhiro Shibayama. "Evaluation of Mesh Size in Model Polymer Networks Consisting of Tetra-Arm and Linear Poly(ethylene glycol)s", . *Gels*, 4(2):50 – 12, 2018-06.

[63] Mingjiang Zhong, Rui Wang, Ken Kawamoto, Bradley D Olsen, and Jeremiah A Johnson. "Quantifying the impact of molecular defects on polymer network elasticity", . *Sci.*, 353(6305):1264 – 1268, 09 2016.

[64] J.-Z. Xue, D. J. Pine, S. T. Milner, X.-l. Wu, and P. M. Chaikin. "Nonergodicity and light scattering from polymer gels", . *Phys. Rev. A*, 46(10):6550–6563, 1992.

[65] Eriko Sato Matsuo, Michal Orkisz, Shao-Tang Sun, Yong Li, and Toyoichi Tanaka. "Origin of Structural Inhomogeneities in Polymer Gels", . *Macromolecules.*, 27:6791 – 6796, 1994.

[66] C Goren, Y Rabin, M Rosenbluh, and Y Cohen. "Elastic Recovery of Gels on Mesoscopic Length Scales. A Photon Correlation Spectroscopy Study", . *Macromolecules.*, 33:5757 – 5759, 2000.

[67] J C Dainty. *Laser Speckle and Related Phenomena*, volume 9 of *Springer-Verlag Berlin Heidelberg*. Springer-Verlag Berlin Heidelberg, 1975.

[68] Ferenc Horkay, Kengo Nishi, and Mitsuhiro Shibayama. "Decisive test of the ideal behavior of tetra-PEG gels", . *The J. Chem. Phys.*, 146(16):164905 – 9, 04 2017.

[69] Jan Skov Pedersen and Peter Schurtenberger. "Scattering functions of semidilute solutions of polymers in a good solvent", . *J. Polym. Sci. Part B: Polym. Phys.*, 42(17):3081 – 3094, 07 2004.

[70] Iwao Teraoka. *POLYMER SOLUTIONS.* Wiley-Interscience. Wiley-Interscience, 2002.

[71] P G De Gennes. *Scaling Concepts in Polymer Physics.* Cornell University Press. Cornell University Press, 1979.

[72] Andre Guinier and Gerard Fournet. *Guinier, Fournet, Small Angle Scattering of X-Rays.* JOHN WILEY S SONS, Inc. JOHN WILEY S SONS, Inc., 1955.

[73] Mitsuhiro Shibayama, Tomohisa Norisuye, and Shunji Nomura. "Cross-link

Density Dependence of Spatial Inhomogeneities and Dynamic Fluctuations of Poly(N-isopropylacrylamide) Gels", . *Macromolecules.*, 29(27):8746 – 8750, 1996-01.

[74] Cyrille Rochas and Erik Geissler. "Measurement of Dynamic Light Scattering Intensity in Gels", . *Macromolecules.*, 47:8012 – 8017, 2014.

[75] Mitsuhiro Shibayama, Yoshihiro Fujikawa, and Shunji Nomura. "Dynamic Light Scattering Study of Poly(N-isopropylacrylamide- co-acrylic acid) Gels", . *Macromolecules.*, 29(20):6535 – 6540, 1996-01.

[76] J Rauch and W Köhler. "Collective and thermal diffusion in dilute, semidilute, and concentrated solutions of polystyrene in toluene", . *The J. Chem. Phys.*, 119(22):11977 – 11988, 12 2003.

[77] K J Zhang, M E Briggs, R W Gammon, J V Sengers, and J F Douglas. "Thermal and mass diffusion in a semidilute good solvent-polymer solution", . *The J. Chem. Phys.*, 111(5):2270 – 2282, 1999-08.

[78] Ute Zettl, Sebastian T Hoffmann, Felix Koberling, Georg Krausch, Jorg Enderlein, Ludger Harnau, and Matthias Ballauff. "Self-Diffusion and Cooperative Diffusion in Semidilute Polymer Solutions As Measured by Fluorescence Correlation Spectroscopy", . *Macromolecules.*, 42:9537 – 9547, 11 2009.

[79] Wyn Brown and Kell Mortensen. "Comparison of correlation lengths in semidilute polystyrene solutions in good solvents by quasi-elastic light scattering and small-angle neutron scattering", . *Macromolecules.*, 21(2):420 – 425, 1988-03.

[80] Peter Schurtenberger, Roger Scartazzini, Linda J Magid, Martin E Leser, and Pier Luigi Luisi. "Structural and dynamic properties of polymer-like reverse micelles", . *The J. Phys. Chem.*, 94:3695 – 3701, 1990.

[81] Peter Schurtenberger and Carolina Cavaco. "Polymer-like lecithin reverse micelles. 1. A light scattering study", . *Langmuir*, 10:100 – 108, 1994.

[82] M Muthukumar and S F Edwards. "Screening concepts in polymer solution dynamics", . *Polym.*, 23:345 – 348, 1982.

[83] Jacques G. H. Joosten, Erik T. F. Geladé, and Peter N. Pusey. "Dynamic light scattering by nonergodic media: Brownian particles trapped in polyacrylamide gels", . *Phys. Rev. A*, 42(4):2161–2175, 1990.

[84] H Z Cummins and E R Pike. *Photon Correlation Spectroscopy and Velocimetry.* Plenum Press. Plenum Press, 1977.

[85] H Benoit, M Benmouna, and Wen Li Wu. "Static scattering from multicomponent polymer and copolymer systems", . *Macromolecules.*, 23(5):1511 – 1517, 1990-09.

[86] J S Higgins and H Benoit. *Polymers and Neutron Scattering.* Oxford University Press. Oxford University Press, 1994.

[87] H. Benoit. "On the effect of branching and polydispersity on the angular distribution of the light scattered by gaussian coils", . *J. Polym. Sci.*, 11(5):507–510,

05 1953.

[88] Masashi Ohira, Yui Tsuji, Nobuyuki Watanabe, Ken Morishima, Elliot P. Gilbert, Xiang Li, and Mitsuhiro Shibayama. "Quantitative Structure Analysis of a Near-Ideal Polymer Network with Deuterium Label by Small-Angle Neutron Scattering", . *Macromolecules.*, 53(10):4047–4054, 05 2020.

[89] Kell Mortensen, Anine L Borger, Jacob J K Kirkensgaard, Christopher J Garvey, Kristoffer Almdal, Andriy Dorokhin, Qian Huang, and Ole Hassager. "Structural Studies of Three-Arm Star Block Copolymers Exposed to Extreme Stretch Suggests a Persistent Polymer Tube.", . *Phys. Rev. Lett.*, 120(20):207801, 05 2018.

[90] Dale S Pearson. "Scattered Intensity from a Chain in a Rubber Network", . *Macromolecules.*, 10(3):696–701, 1977.

List of Publlifications

【Publications related to this thesis】
1. Y. Tsuji, S. Nakagawa, C. I. Gupit, M. Ohira, M. Shibayama, and X. Li, "Selective Doping of Positive and Negative Spatial Defects into Polymer Gels by Tuning the Pregel Packing Conditions of Star Polymers.", Macromolecules, 2020, 53 (17), 7537-7545.
2. M. Ohira, Y. Tsuji, N. Watanabe, K. Morishima, E. Gilbert, X. Li and M. Shibayama. "Quantitative structure analysis of near-ideal polymer network with deuterium label by small angle neutron scattering", Macromolecules, 2020, 53 (17), 4047-4054.
3. X. Li, S. Nakagawa, Y. Tsuji, N. Watanabe and M. Shibayama. "Polymer Gel with a Flexible and Highly Ordered Three-Dimensional Network Synthesized via Bond Percolation", Sci. Adv., 2019, 5, eaax8647.

【Publications not related to the thesis】
1. Y. Tsuji, M. Shibayama*, and X. Li, "Neutralization and Salt Effect on the Structure and Mechanical Properties of Polyacrylic Acid Gels under Equivolume Conditions.", Gels, 2021, 7 (2), 69.
2. Y. Tsuji X. Li and M. Shibayama. "Evaluation of Mesh Size in Model Polymer Networks Consisting of Tetra-Arm and Linear Poly(ethylene glycol)s", Gels, 2018, 4, 50.

Acknowledgements

First, I would like to express my appreciation to my supervisors, Profesor Mitsuhiro Shibayama and Profesor Osamu Yamamura, for their continuous support and helpful suggestions. Without their thoughtful support, I would not accomplish my doctoral works.

Moreover, I got generous support from my colleagues and collaborator. Significantly, Associate Profesor Xinag Li, who is my mentor, gave me a lot of research advice and taught me how I should take an attitude for conducting research. Mr. Caidric Indaya Gupit and Mr. Masashi Ohira also help me with experiments.

I would like to acknowledge the valuable discussion by Assistant Professor Shintaro Nakagawa. Additionally, I would like to thank Associate Profesor Koichi Mayumi, Dr. Yusuke Yasuda, and Mr. Takeyoshi Masumoto for constructive discussion about molecular dynamics simulation. About the mechanical properties of gels, I would like to thank Senior Lecturer Takuya Katashima for the helpful discussion.

The neutron scattering experiment was conducted with TAIKAN BL15 (SANS experiment, 2019B0305) and DNA BL02 (QENS experiment, 2019B0331) at Materials and Life Science Experimental Facility (MLF) at the Japan Proton Accelerator Research Complex (J-PARC) in Tokai, Japan. I would like to thank Dr. Hiroki Iwase, Dr. Shinichi Takata, and Dr. Takeshi Yamada for their technical supports.

The X-ray experiment was conducted with BL-6A and BL-10C (2019G055 and 2021G135) at Photon Factory, High Energy Accelerator Research Organization, KEK in Tsukuba, Japan. I would like to thank Dr. Noriyuki Igarashi and Dr. Nobutaka Shimizu for the technical support to conduct experiments.

I also acknowledge the financial support, Advanced Leading Graduate Course for Photon Science, Program for Leading Graduate Schools (ALPS), and Research Fellowships for Young Scientists (DC2), from Japan Society for the Promotion of Science. Without this financial support, I could not choose a doctoral career. Also, the part of my work was supported by the Sasakawa Scientific Research Grant from

The Japan Science Society. I acknowledge their support.

Finally, I would like to thank my parents for their understanding and cooperation.